

**Micro-Additive Manufacturing of Metal-Oxide-Semiconductor Based Gas
Sensors for Diabetes Detection via Breath Analysis**

by

Manyou Sun

A thesis

presented to the University of Waterloo

in fulfillment of the

thesis requirement for the degree of

Master of Applied Science

in

Chemical Engineering

Waterloo, Ontario, Canada, 2021

©Manyou Sun 2021

Author's declaration

I hereby declare that I am the sole author of this thesis. This is a true copy of the thesis, including any required final revisions, as accepted by my examiners.

I understand that my thesis may be made electronically available to the public.

Abstract

Additive manufacturing (AM) is arousing more and more interest due to its flexibility to produce complex geometry, low fabrication cost and high material compatibility compared with conventional manufacturing. As a micro-scale additive manufacturing technique, aerosol jet printing (AJP) is able to fabricate fine structures with the size of several microns on substrates with flexible shapes. Compared with other thin film technologies, aerosol jet printing is suitable to fabricate thin film microelectronics with complex geometry without creating and removing a mask. One of the most important applications for aerosol jet printing is fabrication of sensors including gas sensors.

Diabetes is a chronic disease which needs continuous monitoring of blood glucose level. Breath acetone analysis is a potential non-invasive technique to monitor blood glucose level without pricking the finger with a lancet. For testing acetone vapor concentration, metal-oxide-semiconductor (MOS) based gas sensor is suitable for this application because of its small size and portability compared with huge equipment in the hospitals.

In this thesis, a metal oxide semiconducting gas sensor based on tin oxide thin film is fabricated which could be used for detection of acetone vapor. The material is synthesized via the sol gel process. The characterization of the material is based on the thin film coated with the sol gel solution. The whole sensor is fabricated via aerosol jet printing technique and the printed sensor is tested in a home-made chamber. Preliminary findings in the thesis prove that aerosol jet printing is another

technique which may be suitable to fabricate gas sensors besides current common techniques such as chemical vapor deposition.

Acknowledgements

At first, I would like to express my sincerest gratitude to both of my supervisors, Professor Boxin Zhao in Department of Chemical Engineering and Professor Ehsan Toyserkani in Department of Mechanical and Mechatronics Engineering. Thank you for providing me the chance to conduct the research and offering me valuable suggestions during my master's study.

Then, I would like to acknowledge all the group members in Surface Science and Bio-nanomaterials Laboratory. Thank you for helping me through the hardest time and cheering me up during COVID pandemic.

I am supported by many cute and warm people in Multi-Scale Additive Manufacturing Lab (MSAM) as well. Thank you for making me feel the warmth, the love and the light in life.

Last but not the least, I would like to thank my family for their support. Thank you for always being here with me.

Table of contents

Author's declaration.....	ii
Abstract.....	iii
Acknowledgements.....	v
List of figures.....	x
List of tables.....	xiii
Chapter 1 Introduction.....	1
1.1 Motivation.....	2
1.2 Research challenges.....	3
1.3 Objectives and goals.....	5
1.4 Research steps.....	5
1.5 Thesis layout.....	6
Chapter 2 Literature review.....	7
2.1 Aerosol jet printing.....	8
2.1.1 General background of additive manufacturing.....	8
2.1.2 General background and working principles of aerosol jet printing.....	9
2.1.3 Related research of aerosol jet printing in literatures.....	13
2.2 Metal oxide semiconducting gas sensors.....	16
2.2.1 General background of gas sensors.....	16
2.2.1.1 Roles and applications for gas sensors.....	16
2.2.1.2 Classifications of gas sensors.....	17
2.2.1.3 Important sensor parameters and requirements.....	19

2.2.2 Metal-oxide semiconducting gas sensors.....	19
2.2.2.1 Sensing mechanisms.....	19
2.2.2.2 Sensor package and structures.....	24
2.2.2.3 Semiconducting materials for gas sensors.....	25
2.2.3 Literature review of tin oxide gas sensors in acetone detection.....	26
2.3 Sol gel technology.....	27
2.3.1 Introduction to sol gel technology.....	27
2.3.2 Sol gel process.....	29
2.3.2.1 Precursors.....	31
2.3.2.2 Hydrolysis and condensation.....	31
2.3.2.3 Gelation / Polymerisation.....	33
2.3.2.4 Syneresis / Aging.....	34
2.3.2.5 Drying.....	34
2.3.3 Sensors derived from sol gel technology.....	35
2.4 Diabetes detection via breath analysis.....	36
2.4.1 Medical diagnosis and human breath.....	36
2.4.2 Breath acetone and blood glucose level.....	39
2.4.3 Current detection technologies.....	43
Chapter 3 Preparation and characterization of sensing material.....	46
3.1 Material selection.....	47
3.2 Material preparation.....	47
3.3 Material characterization.....	50

3.3.1 Surface morphology (SEM).....	50
3.3.2 Crystal structure (XRD).....	50
3.3.3 Optical Properties (UV-Vis).....	51
3.4 Sol-to-gel transition.....	52
3.5 Sensing performance.....	54
3.5.1 Testing chamber setup.....	54
3.5.2 Sample preparation for testing.....	58
3.5.3 Semiconducting behavior and sensing performance.....	59
3.5.3.1 Current-voltage (I-V) characterization.....	59
3.5.3.2 Resistance change with temperature.....	60
3.5.3.3 Dynamic response.....	61
3.5.3.4 Influencing factors on repeatability and reproducibility.....	63
3.6 Summary.....	66
Chapter 4 Aerosol jet printing of the gas sensor package.....	68
4.1 Printing system.....	69
4.2 Process flow.....	70
4.3 Ink formulation.....	71
4.4 Important printing parameters.....	73
4.5 Post treatment process.....	77
4.6 Characterization of printed parts.....	78
4.6.1 Electrodes.....	78
4.6.2 Micro-hotplates.....	82

4.6.3 Sensing layers.....	84
4.7 Summary.....	87
Chapter 5 Summary and recommendations.....	89
5.1 Thesis summary.....	90
5.2 Achievements and disadvantages.....	91
5.3 Recommendations.....	93
Letter of copyright permission.....	94
References.....	96

List of figures

Figure 1 Project flow chart.....	6
Figure 2 Process chart for rapid prototyping [2].....	8
Figure 3 Schematic illustration of an aerosol jet printing system [5].....	10
Figure 4 Schematic illustration for ultrasonic atomization [6].....	11
Figure 5 Detailed illustration of aerosol gas stream and sheath gas stream in the deposition nozzle [7].....	12
Figure 6 Printing parameter for aerosol jet printing [6][8].....	12
Figure 7 Applications for aerosol jet printing [6].....	13
Figure 8 Energy band bending of metal oxide due to oxygen adsorption [28]....	21
Figure 9 Energy level change of a metal oxide (a) before and (b) after VOC exposure [29].....	22
Figure 10 Impacts on relative size between grain size and depletion layer size on sensitivity [30].....	23
Figure 11 Structure of metal oxide semiconducting gas sensor.....	24
Figure 12 Process schematic of sol gel technology.....	30
Figure 13 Hydrolysis of silicon alkoxide catalyzed by acid [52].....	32
Figure 14 Hydrolysis of silicon alkoxide catalyzed by base [52].....	32
Figure 15 Condensation of silicon alkoxide catalyzed by acid [52].....	33
Figure 16 Condensation of silicon alkoxide catalyzed by base [52].....	33
Figure 17 Shrinkage modes for wet gels [54].....	34
Figure 18 Physiological path of acetone production from fatty acids.....	40

Figure 19 Experimental setup for synthesizing tin oxide sol.....	48
Figure 20 Stable tin oxide sol.....	48
Figure 21 Dip coating setup (A tensile tester with z-axis motorized stage).....	49
Figure 22 Surface morphology of the sensing layer.....	50
Figure 23 XRD pattern of tin oxide thin film.....	51
Figure 24 Transmittance of coated tin oxide thin film (after annealing at 450 °C)	52
Figure 25 Mechanisms for epoxide-assisted gelation.....	53
Figure 26 Tin oxide gel prepared from tin oxide sol.....	54
Figure 27 Process for measuring chamber volume.....	55
Figure 28 Picture of home-built sensor testing chamber.....	56
Figure 29 Graphic demonstration of testing system.....	56
Figure 30 Lead attachment on the sensor pad.....	59
Figure 31 I-V curve for tin oxide sensing layer.....	60
Figure 32 Resistance change with temperature during heating for the first time	61
Figure 33 Dynamic response curve for printed acetone sensor.....	62
Figure 34 Linear relationship between sensor response and acetone concentration	62
Figure 35 Comparison of sensor response for replicating samples.....	65
Figure 36 Comparison of sensor response for the same sample.....	66
Figure 37 Optomec M ³ D structure.....	69
Figure 38 Process flow for printing a gas sensor.....	71

Figure 39 Picture of tin oxide ink made from tin oxide sol.....	72
Figure 40 Effects of atomizer gas flowrate on printed line morphology with fixed sheath gas flowrate at 30 cc/min and printing speed at 1 mm/sec.....	74
Figure 41 Effects of sheath gas flowrate on printed line morphology with fixed atomizer gas flowrate at 15 cc/min and printing speed at 1 mm/sec.....	75
Figure 42 Effects of printing speed on printed line morphology with fixed atomizer gas flowrate at 15 cc/min and sheath gas flow rate at 30cc/min...	76
Figure 43 Relationship between line width and printing parameters.....	77
Figure 44 CAD pattern and optical images of electrodes with different trace gaps	79
Figure 45 Optical images and surface profile of the conductive traces.....	80
Figure 46 Connected traces under small designed trace gaps.....	81
Figure 47 A smooth silver surface with a roughness of $0.20 \mu\text{m} \pm 0.01 \mu\text{m}$	81
Figure 48 Differences between uncontrolled sintering and controlled sintering.	82
Figure 49 Micro-hotplate printed by silver ink with larger gaps.....	83
Figure 50 Micro-hotplate printed by silver ink with smaller gaps.....	83
Figure 51 SEM image of the micro-hotplate after applying voltage.....	84
Figure 52 Printed sensing layer with designed gap of (a) $10 \mu\text{m}$ and (b) $5 \mu\text{m}$...	85
Figure 53 Cellphone picture of printed sensing layers on a glass slide.....	85
Figure 54 Optical image of sensing material after heat treatment.....	86
Figure 55 Printed sensing layer on the electrode with trace gap of $50 \mu\text{m}$	86

List of tables

Table 1 Gas sensor applications [25].....	16
Table 2 Sensing materials for resistive-type gas sensors [25].....	25
Table 3 VOCs as biomarkers for disease detection [62][63].....	38

Chapter 1 Introduction

In this chapter, the motivation of the research project presented in this thesis is briefly introduced. Both challenges and problems encountered in the research process and objectives and goals expected to be achieved are described to help the readers better understand the research topic. Finally, the research plan of the project is listed and the structure of the thesis is elaborated.

1.1 Motivation

Diabetes is a chronic disease which needs continuous monitoring of blood glucose level. Currently, the method is to collect a drop of blood by pricking the finger with a lancet and measure the blood glucose level using the blood drop. Although the result is accurate, it is an invasive technique that would cause pain and discomfort to the individuals. Over the past decades, many research projects related to analyzing the relationship between volatile organic compounds (VOCs) and medical diagnosis have appeared and some successful results have been achieved on correlations between breath acetone concentrations and blood glucose levels, which laid the foundation for developing sensing technologies for detection of acetone in human breath for diabetes diagnosis and monitoring.

There are various techniques for breath analysis including gas chromatography mass spectrometry (GC-MS), proton transfer reaction mass spectrometry (PTR-MS), selected ion flow tube-mass spectrometry (SIFT-MS) and so on. These techniques could provide relatively accurate results, but they all have some limitations: GC-MS needs complicated and time-consuming sample preparation procedures, PTR-MS could not distinguish substances with the same molecular weight and SIFT-MS is not able to identify compounds in a mixture of gases. In addition, all of these techniques use bulky and expensive equipment and it requires professional knowledge and specific trainings to operate the machines, and that is why these techniques are not suitable for point-of-care use.

Another way to detect the concentration of specified gas in the breath is the use

of gas sensors, and owing to the development of nanotechnology, nanotechnology enabled sensors possess significant advantages including higher sensitivity and higher selectivity due to the high surface-to-volume ratio of nanostructures and unique chemical, optical and electrical properties. In the past years, chemiresistive sensors based on metal oxide semiconductors have been utilized to detect sub-ppm acetone in human breath. Some recent publications provided evidence for the potential use of metal-oxide-semiconductor based gas sensors for breath acetone detection.

The invention of additive manufacturing, especially inkjet printing and aerosol jet printing, provides a new method for fabrication of electronics including sensors. In this research, aerosol jet printing is used as the printing method for fabricating gas sensors from nanoparticle inks. The whole project includes synthesis of metal oxide nanoparticles, characterization of sensing materials, formulation of nanoparticle ink, aerosol jet printing of gas sensors, and testing of gas sensors. Details would be presented in the next sections.

1.2 Research challenges

Both aerosol jet printing (AJP) and ink jet printing (IJP) are efficient techniques for printed electronics. Although aerosol jet printing has advantages over inkjet printing including the higher printing resolution, a wider range of material selection and the less chance for nozzle clogging, it is truly a newer technique which has a history of less than 20 years. Most of the commercial printed electronics are made with inkjet printing rather than aerosol jet printing. Also, the number of publications on aerosol jet printing is much less than the one on inkjet printing.

For the fabrication of gas sensors, the most common method is chemical vapor deposition in the publication. There are some publications on synthesizing metal oxide nanoparticles and testing the sensing performance, but none of them describes the manufacturing process of the sensor device in details out of the sensing material.

The sensing material used in this thesis is tin oxide synthesized via sol gel process. Sol gel technology is suitable in this project since it is a wet chemical process. Compared with other solid state processes, it is easier to make ink from liquid sol by simply adjusting liquid properties. However, sol gel process is a relatively new technique and is not commonly used in fabricating gas sensors. Thus, how to control the material properties and obtain some sensing signals is the first challenge in this thesis.

The second challenge lies in the ink formulation. For ink jet printing, the only parameter that is important for the ink is its viscosity. Any ink fell in the viscosity range should be printable. However, for aerosol jet printing, the ink should be aerosolized when placed into an ultrasonic atomizer. The mechanism of ultrasonic atomization is not fully understood yet. What kind of ink can be printable still remains an unsolved question for researchers in this field.

How to make the whole fabrication process stable and repeatable is another challenge. From the perspective of material preparation, the condition of the liquid sol varies with time. While for aerosol jet printing process, a small change of the ink would bring significant variances on the printing quality. Therefore, it is important to come out with a standard process for the fabrication.

1.3 Objectives and goals

In this study, the aim is to fabricate a tin oxide acetone sensor which could be used to detect the acetone amount in the environment and also has the potential application on diabetes detection via breath analysis. Thus, the sensitivity of the gas sensor should be high enough to detect the low concentration of acetone vapor. Gas sensors used in medical diagnosis should have the detection limit of sub-ppm level. For the diabetes detection, there are thousands of VOCs and other gases in human breath, selectivity is another important parameter. One of the shortcomings of metal oxide semiconducting gas sensors is that response time is long compared with other types of sensors. Therefore, efforts should be put to trying to shorten the response time to improve the sensing performance. Details about sensor parameters and requirements will be given in Section 2.2.1.3.

1.4 Research steps

The steps included in this thesis are as follows:

1. Sensing material is selected, synthesized and characterized.
2. Testing chamber is designed and built and sensing performance of the sensing material is tested.
3. Aerosol jet printing of the sensor package is conducted including electrodes, micro-hotplates and sensing materials.
4. Post treatment process for aerosol jet printing is studied.
5. Printing quality is monitored and characterized after post treatment process.

Figure 1 shows the project flow chart for this thesis.

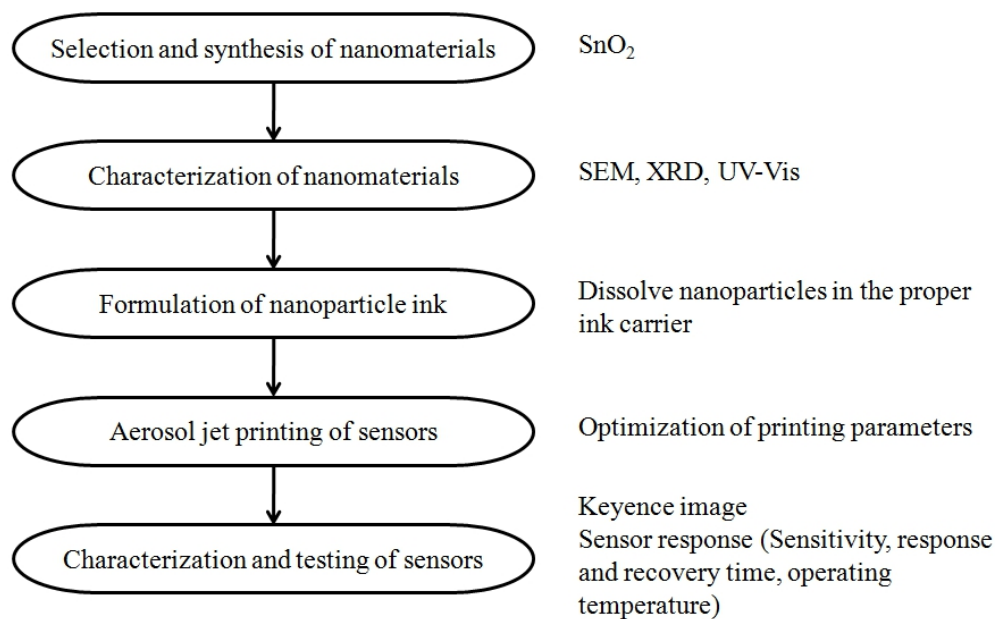


Figure 1 Project flow chart

1.5 Thesis layout

This thesis is divided into 5 chapters. Chapter 1 is the general introduction of the project including motivation, challenges, goals to be achieved and work that has been done in order to realize the goal. Chapter 2 reviews the technologies related to this thesis including aerosol jet printing, metal oxide semiconducting sensors and sol gel technology. Information about breath acetone analysis and diabetes detection are also summarized. In Chapter 3, details about synthesizing and characterizing the sensing material are given. Sensing performance of the material is elaborated in Chapter 3 as well. Fabrication process is explained in Chapter 4. It describes each step included in aerosol jet printing and contains the characterization results of printed parts. Chapter 5 is the summary of this thesis.

Chapter 2 Literature review

The contents in this chapter provide background knowledge and review state-of-the-art developments for related technologies involved in the research project including aerosol jet printing technique, sol gel chemistry, metal oxide semiconducting gas sensors and diabetes detection via breath analysis. Introduction to these technologies, working principles and mechanisms, and applications related to the current research are summarized from all these aspects.

2.1 Aerosol jet printing

2.1.1 General background of additive manufacturing

Additive manufacturing is a CAD (computer-aided design) based process which is used to form a three dimensional near-net-shape part in a layer-upon-layer manner, as opposed to subtractive manufacturing. Compared with traditional manufacturing methods, the advantage of additive manufacturing lies in the reduction of time and money used to fabricate a single product by reducing the material loss and providing an easier fabrication process and meanwhile the ability to produce parts with complex shapes. According to the most recent Wohler's report(Wohler's report 2020) [1], the past decade witnessed the rapid growth on investments of additive manufacturing due to its advantages and promising prospects in manufacturing industry.

All the additive manufacturing technologies could date back to their origin called rapid prototyping, which was invented in 1980s and follows the process shown in Figure 2 [2]. Typically, it is a process with the combination of several technologies, namely, computer-aided design (CAD), computer-aided manufacturing (CAM) and computer numerical control (CNC). Sometimes, after rapid prototyping, it still needs some post-treatments in order to achieve the final product.

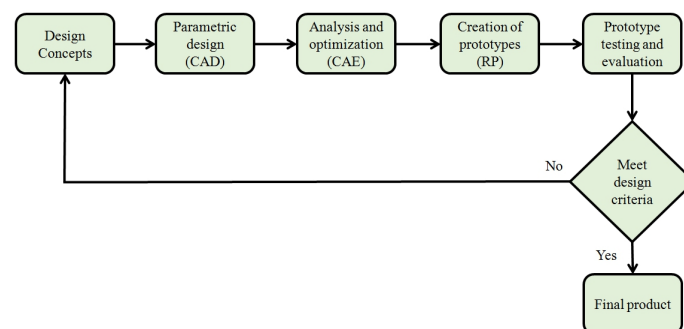


Figure 2 Process chart for rapid prototyping [2]

With decades of development, there are various technologies, both beam-based and non-beam-based methods, included in additive manufacturing. According to ASTM standards, additive manufacturing technologies could be divided into seven classifications [3] including VAT photopolymerisation, material jetting, binder jetting, material extrusion, powder bed fusion, sheet lamination and directed energy deposition. All the technologies included in AM follow the process chart in Figure 2. In the classification of material jetting, there are two techniques, namely inkjet printing and aerosol jet printing. Both of them are suitable for microfabrications of printed electronics. Aerosol jet printing is used as the printing technique in this thesis and details about aerosol jet printing are elaborated in the following subsections.

2.1.2 General background and working principles of aerosol jet printing

Aerosol jet printing technology is a new technique invented and commercialized by Optomec Inc. in the beginning of 21st century. The first publication using aerosol jet printing technique appeared in 2001 [4]. This technique uses liquid ink as the raw printing material. An aerosol gas stream is created by the atomization of liquid ink, compressed and protected by another gas stream called sheath gas stream and deposited directly on the substrate. Figure 3 [5] shows the schematic illustration of an aerosol jet printing system.

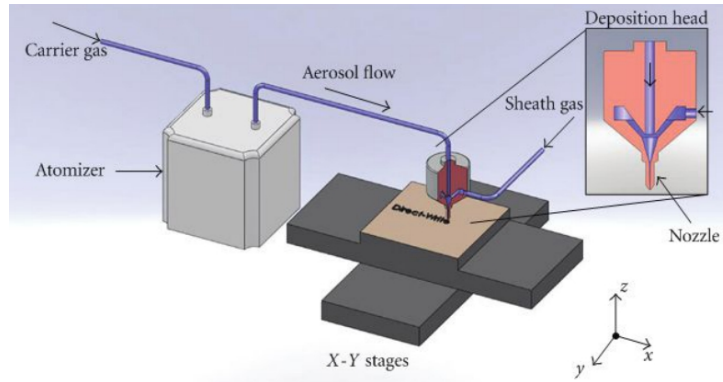


Figure 3 Schematic illustration of an aerosol jet printing system [5]

Theoretically, any materials that could be suspended stably in an aerosol can be considered as candidate materials for aerosol jet printing technique. Compared with inkjet printing, which has a viscosity limit for the ink of below 20 cP, the viscosity of the ink for aerosol jet printing could range from 1 to 1000 cP based on different atomization techniques [6]. There are two atomization techniques for aerosol jet printers: ultrasonic atomization and pneumatic atomization. The printer used in this project uses ultrasonic atomization technique which has an ink viscosity limit of 1-10 cP but is able to produce much more uniform aerosols.

Figure 4 [6] is a schematic illustration of the ultrasonic atomization process. The wave generated by the high-frequency oscillation of the transducer is transferred through the transfer medium (water in this case) to the ink vial, which would generate a standing wave on the surface of the ink, leading to the formation of peaks on the ink surface and the ejection of tiny droplets from the ink due to local shear at the peaks. Then the positive pressure provided by the carrier gas would bring those tiny droplets from the ink vial to the deposition nozzle. The mixture of these tiny droplets and the

carrier gas is called an aerosol jet, and that is why this technique is called aerosol jet printing.

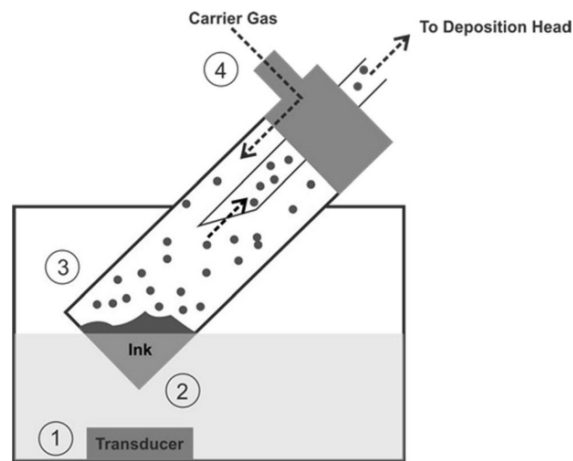


Figure 4 Schematic illustration for ultrasonic atomization [6]

The novelty of aerosol jet printing technique compared with other direct write technologies lies in the introduction of the secondary flow called sheath gas which acts as a virtual deposition nozzle besides the physical deposition head as shown in Figure 5 [7]. The main function of the sheath gas is to focus the aerosol flow. Thus, the most important printing parameter for aerosol jet printing is focusing ratio, the ratio between the volume of aerosol gas and the volume of sheath gas. During aerosol jet printing process, printing performance is able to be adjusted and optimized by changing the focusing ratio. Besides, due to the addition of the sheath gas flow, the probability of nozzle clogging has been decreased compared with nozzles for inkjet printing.

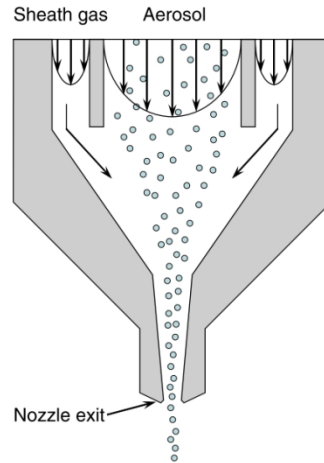


Figure 5 Detailed illustration of aerosol gas stream and sheath gas stream in the deposition nozzle [7]

Some other printing parameters which may influence the printing performance are listed as shown in Figure 6 [6][8]. Among all the research, the minimization of overspray caused by excess inertia of aerosol flow by optimizing printing parameters is the most challenging problem for aerosol jet printing technique.

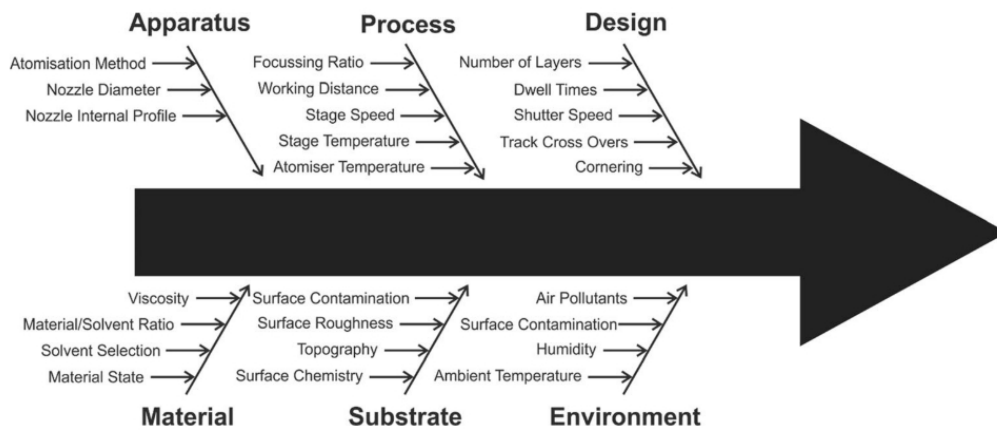


Figure 6 Printing parameter for aerosol jet printing [6][8]

Aerosol jet printing is a technology initially designed specifically for printing electronics and most of the current research projects are related to this field. But with the continuous development and increasing maturity of this technique, it starts to be involved in fabrications in other fields. Figure 7 [6] lists some common applications

for aerosol jet printing. In this project, aerosol jet printing is used to fabricate elements in the sensor package including the sensing material, electrodes and micro-hotplates.

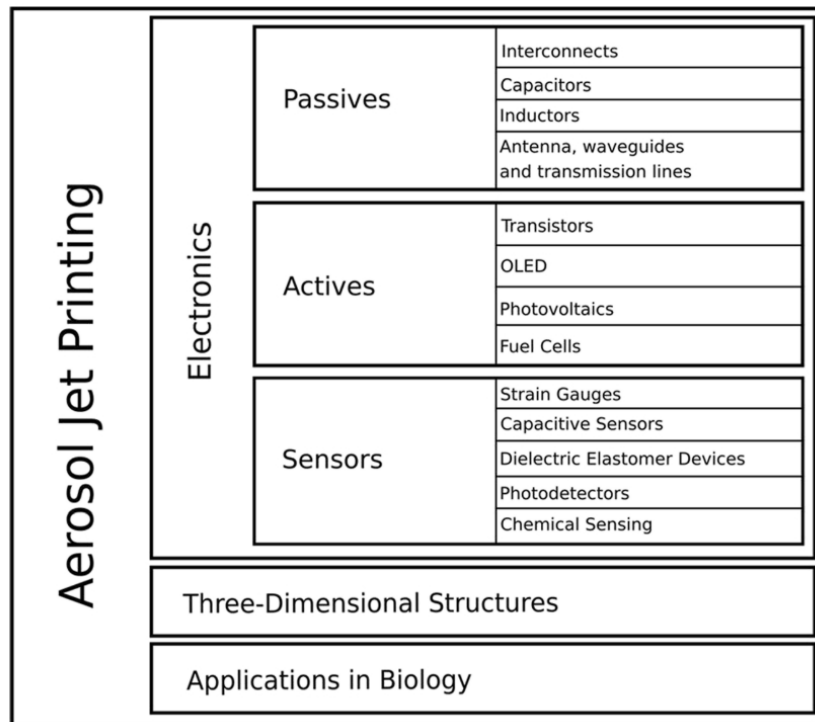


Figure 7 Applications for aerosol jet printing [6]

2.1.3 Related research of aerosol jet printing in literatures

As mentioned before, as a technology existing for 20 years, there are some publications on aerosol jet printing, both from experimental and simulation aspects.

Salary et al. conducted computational fluid dynamics simulations on both pneumatic atomization process [9] and material transport and deposition process [10] in aerosol jet printing, which provide theoretical foundations -- the influence of sheath gas flow rate and aerosol gas flow rate on the line morphology-- for related researchers.

Among all current studies using aerosol jet printing to fabricate sensors, strain sensors account for a large proportion. Agarwala et al. [11] fabricated a silver strain sensor using commercial silver nanoparticle ink on the bandage substrate combined with laser sintering to cure the sensor without damaging the substrate, and the resulting product has great potential for home healthcare usage. In the research work conducted by Fujimoto et al. [12], a capacitance-based strain gauge was printed with silver ink on the flexible Kapton substrate with poly methyl methacrylate (PMAA) as the dielectric layer. The resulted sensor has relatively high sensitivity and gauge factor. Zhao et al. [13] prepared the carbon fiber prepreg and alcohol-based silver ink was printed directly on the prepreg to form the multifunctional composites used as strain sensors. The results prove the high potential of the new technology on manufacturing composite structures.

Compared with strain sensors, there are not too much research on fabricating gas sensors or other chemical sensors using aerosol jet printing. For most of the current studies, aerosol jet printing is not used to fabricate the whole sensor package, but is applied to manufacture some of the parts included in the sensor package such as the electrodes and the heaters [14-17]. Vasiliev et al. [14] printed the tin oxide nanocrystallines as sensing material and platinum nanoparticles to make the micro-hotplate and the resulting package is able to detect carbon monoxide down to 1 ppm and could be stable up to 450 °C. Zhu et al. [15] used aerosol jet printing technology with ultrasonic atomization to fabricate a graphene gas sensor to detect ammonia gas and the sensor has high sensitivity at low gas concentration. Liu et al.

[16] printed the single-walled carbon nanotubes decorated with platinum on the micro-fabricated electrodes on a silicon wafer and tested its sensing response towards hydrogen gas.

Aerosol jet printing can be combined with optical fibers as well to fabricate optical sensors [18-21]. In the work conducted by Alemohammad *et al.* [18][19], a silver thin film with the thickness of less than 10 μm was deposited via aerosol jet printing technique on the optical fiber Bragg grating sensor. The resulted package has concurrent sensitivity towards both temperature and structural strain. In [20] and [21], aerosol jet printing and electroless nickel plating were combined and used to fabricate a micro-scale coating on the optical fiber Bragg grating sensor. Silver layer with 1-2 μm was deposited via aerosol jet printing and electroless nickel plating was used to increase the layer thickness to a desired range. Results show that the bi-material coating is able to increase the sensitivity to force and temperature.

Besides sensors, there are many other applications for aerosol jet printing as well. In [22], aerosol jet printing of silver nanoparticles is used for surface patterning of magnesium in order to improve the cell adhesion, infiltration and proliferation of the biocompatible material. Characterization work is conducted to study the printed structure and the diffusion zone at material interface. Jabari *et al.* [23] explored the feasibility to fabricate graphene interconnects via aerosol jet printing and achieved the optimal printing parameters for the graphene ink. They also studied the sintering procedures for the aerosol jet printed graphene patterns [24].

2.2 Metal oxide semiconducting gas sensors

2.2.1 General background of gas sensors

2.2.1.1 Roles and applications for gas sensors

As its name indicates, a gas sensor is a device designed for detecting the type and measuring the concentration of a specific gas from a gas mixture. According to different situations, gas sensors are designed to satisfy different needs and therefore possess different functions. Gas sensors could be used to detect a relatively small amount of combustible gases such as hydrogen in order to prevent fire disasters from happening. Air quality could be measured and monitored by gas sensors in order that the emission of air pollutants like nitrogen oxides and sulfur oxides could be controlled within a limited amount according to the standard. The amount of breathing gas such as carbon dioxide and oxygen could be detected for the sake of human health. Besides these most common applications, gas sensors are becoming more and more popular in some specific fields including medical science, aerospace, agriculture, power plants, etc. Table 1 [25] summarizes the application fields of gas sensors and desired gases they are aiming at.

Table 1 Gas sensor applications [25]

Examples of application fields	Description	Examples of target gas
Environment	Detection and monitoring the air quality in the environment, especially for toxic industrial gas emissions	VOCs, NO _x , CO, CH ₄ , NH ₃ , H ₂ S
Safety	Detection of combustible and	Combustible gases,

	flammable gases to prevent fires and explosions, including sensors in fire alarms	flammable gases, explosives
Medical	Diagnostic and monitoring of diseases via breath analysis	VOCs, NH ₃ , NO _x
Industry	Process monitoring and waste stream control	HCs, conventional pollutants
Military	Detection of toxic gases and agents	Toxic gases
Aerospace	Monitoring of the concentration of oxygen and flammable gases to prevent explosions	O ₂ , H ₂ , humidity
Agriculture	Testing and monitoring of water and soil quality; Inspection of meat quality	amine, humidity
Power Plant	Control and monitoring the concentration of engine gases in order to optimize the working efficiency	O ₂ , CO, HCs, NO _x , H ₂

2.2.1.2 Classifications of gas sensors

The definition of a sensor is a device that could measure the physical input from the environment and transfer it into some signals that could be detected by human or machines. A gas sensor is a device that could transfer the change of a small amount of gas concentration into some physical quantities that is visible to human's eyes or detectable by some machines. There are more than one way to classify gas sensors,

among which the most popular classification method is based on the working principals of gas sensors. According to different transduction mechanisms for detecting the gas species, gas sensors are divided into optical sensors, electrical sensors, electrochemical sensors, mass-sensitive sensors, calorimetric sensors and magnetic sensors [26].

As their names indicate, different types of gas sensors transform different types of phenomena into signals that could be detected. An optical sensor refers to a device that transform changes of optical phenomena such as the change of absorbance or reflectance of the material, or the stimulation of fluorescence effect when the target gas interacts with sensing materials. Electrochemical sensors are based on electrochemical interactions between gas and electrodes. Mass-sensitive sensors change the mass change at the surface into another property change of the substrate, with piezoelectric devices as a good example. The mechanism of a magnetic sensor lies in the paramagnetic property changes of the analyzing gas. Calorimetric sensors, also called thermometric sensors, transfer the heat effect of a chemical reaction or an adsorption process into the desired signal.

The focus of this project is the fabrication of a metal oxide semiconducting gas sensor, which belongs to the category of electrical sensors. For electrical sensors, during interactions between the gas phase and sensing materials, the electrical signal change, i.e., the change of resistance or electrical current of the sensor, could be detected. Detailed sensing mechanism of metal-oxide-semiconductor-based gas sensors would be presented in Section 2.2.2.

2.2.1.3 Important sensor parameters and requirements

Since the function of a gas sensor is to detect the presence or measure the concentration of a specific gas in a gas mixture, it is significant that the sensor should have real-time and stable output signals which should be able to provide enough and reliable information for analyzing gas compositions when installed in the test environment. Therefore, an ideal gas sensor should possess the following characteristics.

The priority for designing a gas sensor is that the sensor should produce signals which are easy enough to be detected and measured. In another word, the sensor should have high sensitivity to measured gas. A gas sensor should also have high selectivity to the target gas, which means that it should have more response towards the target gas while less response towards the others. The time for the sensor to produce maximal signal upon exposing to the target gas (response time) and the time for the sensor output to return to the original point when separating the sensor and the gas source (recovery time) should be as short as possible. Other than these, high durability, low cost, simple fabrication method and suitable size for specific applications are all important in the gas sensor design.

2.2.2 Metal-oxide semiconducting gas sensors

2.2.2.1 Sensing mechanisms

In order to figure out what factors are important in semiconducting gas sensor research, it is necessary to fully understand the working principles and sensing

mechanisms of this type of sensors. As is mentioned before, metal-oxide-semiconductor-based gas sensors belong to the category of electrical sensors, which means that electrical resistivity of the material would change due to material interactions. In this case, material interactions refer to interactions between oxygen in air atmosphere and the sensing material.

In air ambient, metal oxide semiconductors always show high resistance due to the formation of a depletion layer on the surface. When the metal oxide is exposed to the oxygen in air, oxygen species would be adsorbed on the surface of the metal oxide, usually in the forms of ions including $O_{2(ads)}^-$, $O_{(ads)}^-$ and $O_{(ads)}^{2-}$ according to different temperatures [27]. Upon adsorption on metal oxide surface, owing to the formation of ionic species, oxygen molecules would attract the electrons in the conduction band of metal oxide material and trap them at the surface, leading to formation of holes in the bulk of metal oxide and negative charge accumulation on the surface of the material. The accumulation of negative charge leads to the formation of a depletion region, also called a space-charge layer, which results in bending of energy band and the increase of the material resistivity. Figure 8 [28] is the demonstration of an energy band diagram of a metal oxide after oxygen adsorption.

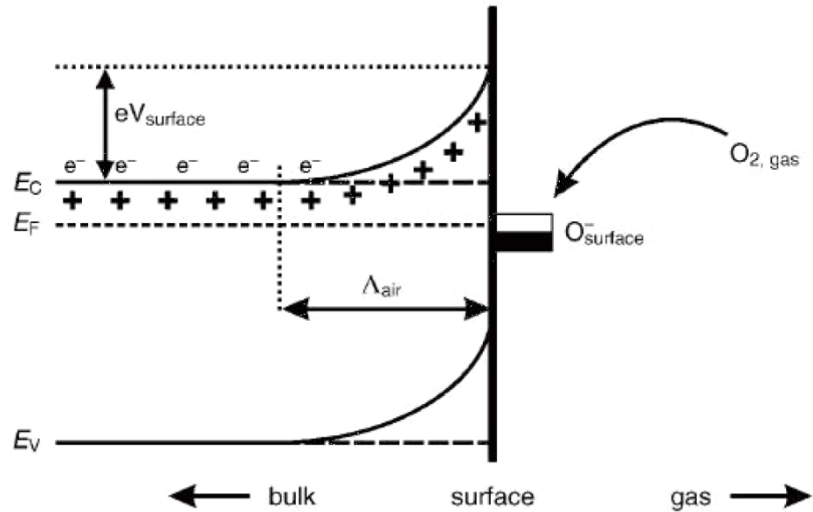


Figure 8 Energy band bending of metal oxide due to oxygen adsorption [28]

When two grains are in close contact, with the appearance of two space-charge layers, an energetic interface called Schottky barrier would form [28]. The conductivity of the metal oxide closely depends on the intensity of the Schottky barrier. When a VOC is adsorbed on the metal oxide surface and reacts with the oxygen species, the intensity of Schottky barrier would be changed which leads to the changes in electrical resistivity. Due to the fact that the extent of change in intensity of the Schottky barrier is positively related to the number of VOC molecules involved in the reaction, it is possible to have different electrical signals when exposing to VOCs under different concentrations. Figure 9 [29] shows the energy level change of a metal oxide before and after exposing to VOCs.

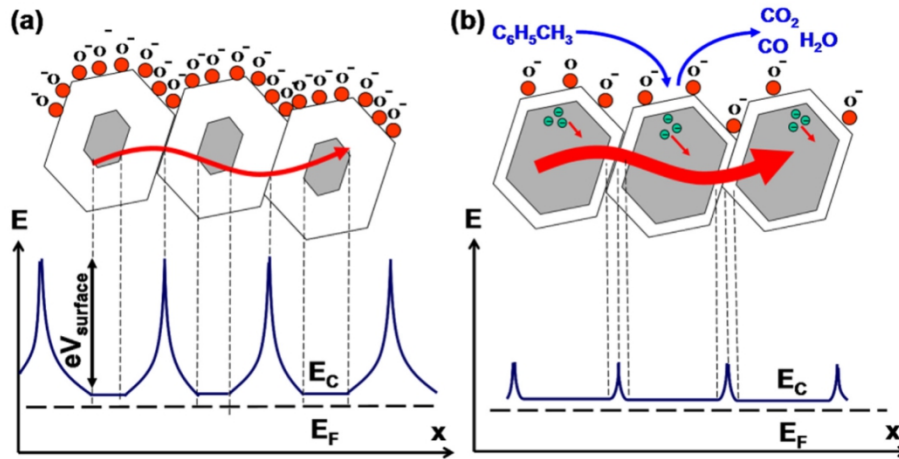


Figure 9 Energy level change of a metal oxide (a) before and (b) after VOC exposure

[29]

Many factors would affect the sensitivity of the sensing material, among which the most important one is the grain size. The relative size of the space-charge layer and the grain size would dramatically influence the sensing performance. There are three scenarios in this case, as shown in Figure 10 [30]. The first one is that when the grain size of sensing material is relatively large ($d \gg 2L$), the resistivity of the material is largely dependent on the electrons in the bulk of the grains, a little modification of the surface charge would not dominate the material properties. Therefore, in this case, the adsorption of VOCs will not make a significant change to the sensing material. The second case is that when the grain size and the thickness of the space-charge layer are close to each other ($d \geq 2L$), the change of the depletion layer begins to affect the material resistivity. The resistivity of the sensing materials changes with exposure to VOCs. At last, when the grain size is smaller than the thickness of depletion region ($d < 2L$), the resistivity change of the metal oxide can be fully considered as the result of the change of surface charge. Thus, a small extent of surface reaction would cause

drastic change in the material resistivity. In other word, the material has high sensitivity towards VOCs in this case.

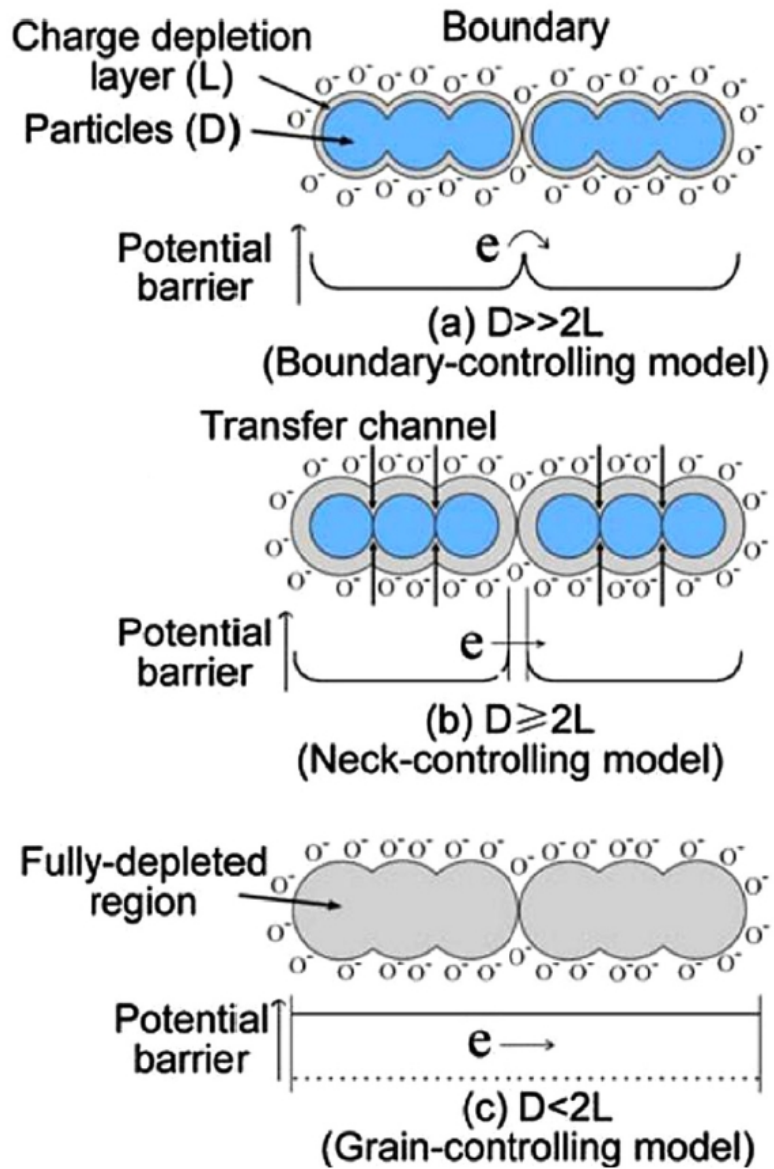
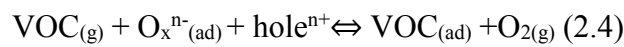
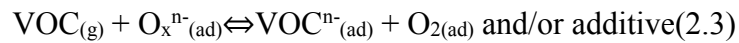
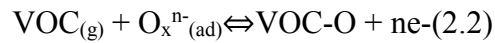
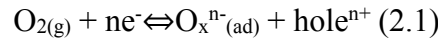


Figure 10 Impacts on relative size between grain size and depletion layer size on sensitivity [30]

Other than grain sizes, other factors could affect the gas sensing performance as well including temperature, humidity and many other external factors. The impact factors are significantly comprehensive and it is still controversial till now, but it is certain that the sensor response largely depends on the measuring environment.

As a summary, the adsorption and reaction of VOCs on the metal oxide surface could be described in the following equations, (2.1) for oxygen adsorption and (2.2) - (2.4) for gas sensing [27]:



2.2.2.2 Sensor package and structures

Typically, a MEMS gas sensor is consisted of a substrate to provide the support for the whole structure, sensing material to detect the gas concentration change and a pair of electrodes in order to form an electrical circuit. Since the optimal operation temperature of the metal oxide semiconductor sensor is always beyond room temperature, a built-in heater is designed on the backside of the substrate in the sensor package. Figure 11 shows a typical structure for a metal-oxide-semiconductor based gas sensor [31].

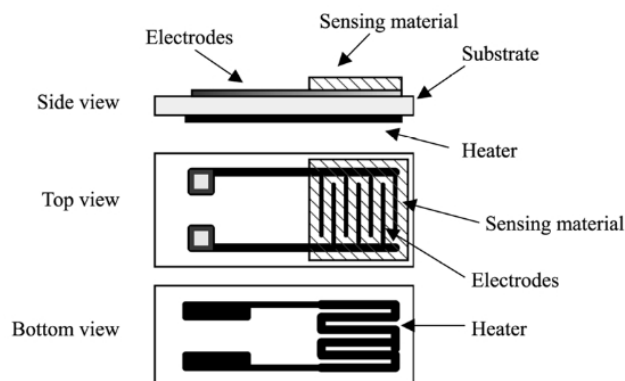


Figure 11 Structure of metal oxide semiconducting gas sensor

(Reprinted with permission from [31])

2.2.2.3 Semiconducting materials for gas sensors

As mentioned before in 2.2.2.1, metal oxide semiconducting materials are most commonly used for making conductometric gas sensors due to their simple structure, easy fabrication and the capability of sensing different gases via easily adjusting the working condition. Table 2 [25] introduces some types of gases that could be detected using semiconductor gas sensors and the types of metal oxide material that are preferred for the listed application.

Table 2 Sensing materials for resistive-type gas sensors [25]

Gas to be detected	Metal oxide materials
Reducing gases	SnO ₂ , CTO, Ga ₂ O ₃ , In ₂ O ₃
Oxidizing gases	In ₂ O ₃ , WO ₃ , ZnO, TiO ₂
Ammonium	WO ₃ , MoO ₃ , In ₂ O ₃
Carbon dioxide	SnO ₂ /La ₂ O ₃ , Al ₂ O ₃ /V ₂ O ₅ , BaTiO ₃ /CuO, BaSnO ₃
Sulfur dioxide	SnO ₂ /CuO, SnO ₂ /Ag ₂ O
Oxygen	Ga ₂ O ₃ , SrTiO ₃ , SrTiFeO ₃ , TiO ₂ , Nb ₂ O ₅ , ZnO
Alcohol	La ₂ O ₃ /In ₂ O ₃ , La ₂ O ₃ /SnO ₂ , In ₂ O ₃ /Fe ₂ O ₃
Humidity	In ₂ O ₃ /SiO ₂ , TiO ₂ /MgCr ₂ O ₄ , SrTiO ₃ , LaFeO ₃

In this project, the aim is to fabricate an acetone gas sensor which could be used to detect acetone vapor at low concentration. Tin oxide nanoparticle is selected as the sensing material for this purpose since acetone vapor is a reducing gas and nanotechnology-based sensors have better sensing performance according to the sensing mechanism stated before.

2.2.3 Literature review of tin oxide gas sensors in acetone detection

In the past three decades, development of semiconducting gas sensors is becoming a more and more popular research topic. Among all the metal oxide materials, tin oxide attracts lots of attention because of its wide band gap of 3.6 eV and its unique and tunable properties including electrical property which is important for gas sensor research. Considerable studies on fabricating acetone sensors based on tin oxide have been appeared. Numerous methods have been tested in order to improve the sensitivity and lower the detection limit of tin oxide towards acetone vapor, including doping with impurities, modifying the particle morphology and preparing composite materials from tin oxide [32].

In [33], Zhang et al. prepared Co_3O_4 -loaded SnO_2 composite and used screen printing to manufacture a thick film sensor. The results show that when the molar ratio of the dopant reaches 5%, the sensitivity of the sensor (defined by ratio between resistance under air ambient R_a and resistance under target gas environment R_g) is largely increased to 235 for 1000 ppm acetone at 300 °C, which is around 5 times compared with pure SnO_2 thick film. In [34], Zhang et al. synthesized mulberry-shaped SnO_2 structures and loaded samarium oxide on them. With 2.5% molar ratio of samarium oxide loading, the sensitivity increased by 2.5 times and the detection limit to acetone vapor reduced from 500 ppb to 100 ppb.

Efforts have been put into morphology modification of nanostructures in order to improve the tin oxide sensing performance as well. Ma et al. [35] synthesized hollow tin oxide nanobelts via capillary electrospinning and the resulted nanobelts have the

sensitivity R_a/R_g up to 6.7 when exposing to 5 ppm of acetone vapor and its response time and recovery time are short enough, about 38 s and 5 s respectively. Multishelled SnO_2 hollow microstructure is also synthesized by the same research group [36] with carbon microspheres as the template for synthesis. The sensor response R_a/R_g ranges from 28.7 to 653 when exposing to acetone vapor from 50 to 3000 ppm at 200 °C. Wang et al. [37] developed a 3D hierarchical tin oxide nanoflowers via a template-free hydrothermal method. The response R_a/R_g to 50 ppm acetone vapor is 29.2 at 170 °C and its detection limit is under 5 ppm.

In this project, sol gel technology is used to synthesize tin oxide material and aerosol jet printing is applied to deposit the material and fabricate the sensor package. The introduction to sol gel technology is in the following section.

2.3 Sol gel technology

2.3.1 Introduction to sol gel technology

Given the fact that developing materials with complex functionality is becoming more and more important in modern science and engineering, exploring various synthesis methods has become a prevalent research topic. For preparing metal oxide materials, the most common way is to mix the corresponding metal powder materials and achieve the desired metal oxide via heating the metal powders. This solid state reaction is easy to achieve due to the maturity of furnace technology, but conversion rate of the reaction is not high enough since oxidation reactions only take place at the surface of the material. Ball-milling could be used to decrease the particle size to

increase the conversion rate of the reaction. However, it would make the process more complicated and therefore require more energy. Typically, for solid state synthesis of metal oxide particles, the reaction temperature is always high and it is difficult to control the particle morphology as well.

Researchers have put many efforts into developing better synthesis methods for metal oxide particles, trying to solve the problems with solid state reactions. Several wet chemical ways appeared including solvothermal synthesis, thermal decomposition, microwave-assisted synthesis, coprecipitation, sol-gel method, etc [38][39]. Among them, sol gel technology has aroused many interest because of its lower reaction temperature and simple reaction process.

In mid-1800s, Ebelman [40] prepared the first metal alkoxide by mixing SiCl_4 and alcohol and found that the mixture turned from liquid to gel after exposure to atmosphere for a period of time, which laid the foundation of developing sol gel technology. However, in the following century, this phenomenon only attracted the interest of the chemists [41]. Until 1930s, Geffcken realized that this process could be used for preparing metal oxide thin film [42]. Since then, more and more publications on sol gel chemistry have emerged.

The structure of inorganic gels prepared from metal aqueous salts has been discussed for decades. In 1864, Graham [43] demonstrated that water content in silica gel could be replaced by other organic solvent, which implied that solid skeleton and continuous porosity are consisted in the gel structure. This hypothesis was widely accepted by researchers until 1937, in that year, Hurd [44] published an article

demonstrating the forming mechanism of silica gels and showing that silica gels should be composed of a polymeric solid network surrounded by the continuous liquid phase.

In mid and late 20th century, both mining industry and ceramics industry began to be interested in sol gel science. Roy et al. synthesized homogeneous powder of various novel metal oxides via sol gel method containing Al, Si, Ti, Zr and other elements that cannot be synthesized via conventional solid state reactions [45][46]. In 1971, Dislich [47] developed multicomponent glasses by hydrolysis and condensation of metal alkoxide and provided an alternative method for fabricating multicomponent oxide glasses at a lower temperature without passing through the molten phase. In 1970s, several companies submitted the patents on making commercial ceramic fibers out of metalorganic precursors [48]. Yoldas [49] demonstrated the possibility of fabricating ceramic monolith by gelation of metal organic precursors and carefully drying the gel. The possibility of making bricks or windows at room temperature has attracted many researchers around the world.

In the past 30 years, sol gel technology has been explored from more aspects and more and more applications have been found. Steps involved in the sol gel technology will be elaborated in the next section.

2.3.2 Sol gel process

Sol gel technology is a method for synthesizing metal oxide ceramics starting from small molecules, also known as precursors. It begins with hydrolysis and condensation of precursor molecules to form the sol, passes through the formation of

the solid network structure containing a liquid medium called the gel and ends in the removal of the liquid medium. According to International Union of Pure and Applied Chemistry (IUPAC), a sol is defined as 'a fluid colloidal system of two or more components' [50], while a gel is a 'non-fluidic colloidal network or polymer network that is expanded throughout its whole volume by a fluid' [51]. According to this definition, particles ranging from 1 nm to 1 μm dispersed in a liquid medium can be called a sol, and a gel refers to the system consisted of continuous solid network and liquid phase. Several steps are included in the sol gel process, including the formation of the sol from partial hydrolysis and condensation of the metal alkoxide precursors, formation of the gel via polycondensation, syneresis or 'aging' of the gel and finally drying the gel to form either xerogel or aerogel. Figure 12 is a summary graph of processes involved in sol gel technology and details in each step will be explained in the following subsections [48].

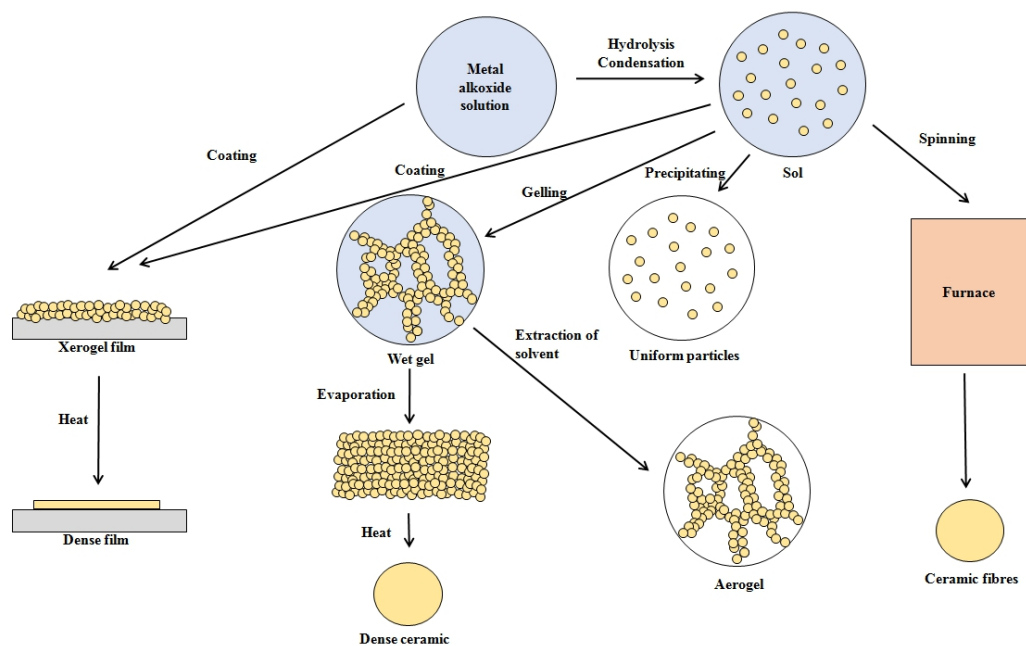


Figure 12 Process schematic of sol gel technology

2.3.2.1 Precursors

The most common type of precursors for sol gel technology is the metal alkoxide, with the formula of $M(OR)_z$, where M represents for a metal element with +z valence and R stands for the alkyl group. In order to achieve metal alkoxides in sol gel process, metal chlorides are always used for the preparation. For elements with high electronegativity, the reaction between the chloride and the alcohol could produce the corresponding metal alkoxide following equation (2.5):



For other metal elements, a base such as ammonium should be added for the reaction to happen, see equation (2.6):



When preparing metal alkoxides from metal chloride, the selection of alcohol type is significant. For alcohols with straight chains and lower carbon numbers, it undergoes the direct substitution reaction and form the desired product. However, if the alcohol is with complex chains, side reactions may occur, leading to the side product and lower yield.

2.3.2.2 Hydrolysis and condensation

The first step in the sol gel process is the hydrolysis and condensation reaction of the precursor in order to complete the transition from the precursor to the sol. Once the liquid precursor is ready, the addition of any amount of water will start the hydrolysis. During hydrolysis, the alkoxy group connected to the metal center will be

replaced by the hydroxyl group, passing through a pentacoordinate transition state under both acidic and basic condition. According to different ratios between water and precursor molecules, more than one alkoxy groups could be replaced. Figure 13 and Figure 14 [52] show schemes for hydrolysis reaction catalyzed by acid and base respectively.

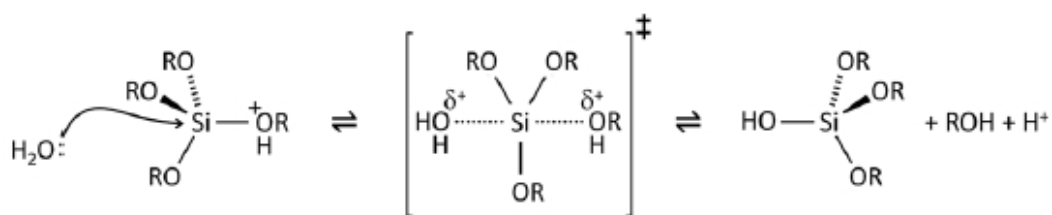


Figure 13 Hydrolysis of silicon alkoxide catalyzed by acid [52]

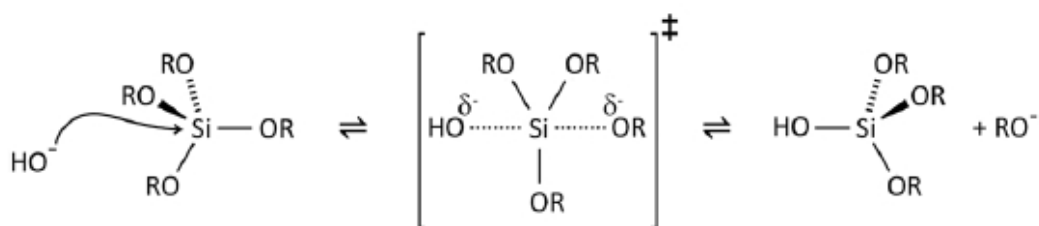


Figure 14 Hydrolysis of silicon alkoxide catalyzed by base [52]

Similar to hydrolysis, condensation is catalyzed by either acid or base and results in the formation of the bond between metal or silicon and oxygen. The degree of condensation would depend on the degree of hydrolysis that has already occurred. In acidic and basic conditions, the relative rate of hydrolysis and condensation are different, which leads to different gel morphology after gelation. In basic conditions, condensation occurs after the completion of hydrolysis, resulting in multiple condensation steps at the same time and thus the formation of highly branched molecules. However, in acidic conditions, hydrolysis on the terminal hydroxyl group

is the fastest. Therefore, condensation prefers to occur on the terminal group forming molecules with chain structures. Figure 15 and Figure 16 [52] show schemes for condensation reaction catalyzed by acid and base.

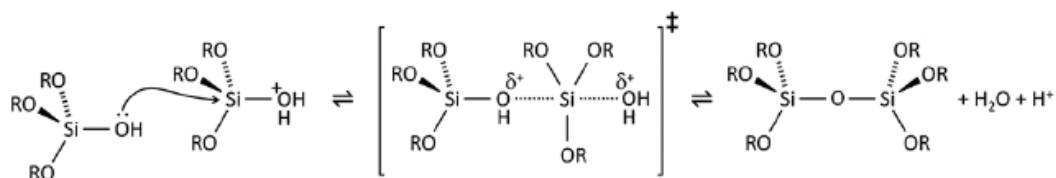


Figure 15 Condensation of silicon alkoxide catalyzed by acid [52]

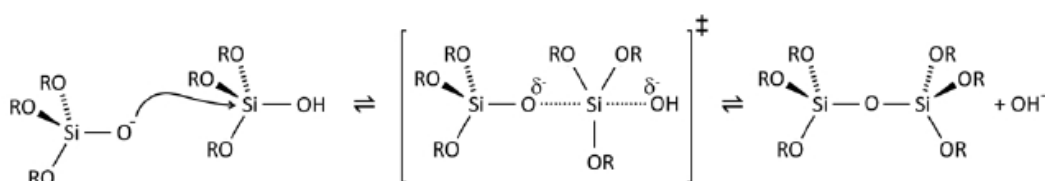


Figure 16 Condensation of silicon alkoxide catalyzed by base [52]

2.3.2.3 Gelation / Polymerisation

With the hydrolysis and condensation reaction continuing, the already formed clusters grow until they begin to approach one another and gelation occurs by linking these clusters via a percolation process. The gelation point refers to the time point when the largest cluster reach across the whole container. Before the gelation, the material in the container is a flowing liquid, while after the gelation point, the material stays stationary even if the container is tilted. Owing to different hydrolysis and condensation mechanisms in acidic and basic conditions as stated before, different gel structures would form when catalyzed by acid and base. If the system is catalyzed by an acid, chain-like molecules crosslink and form the gel with the network structure called a polymeric gel. If the system is catalyzed by a base, highly branched

molecules crosslink to form the gel called a colloidal gel [53].

2.3.2.4 Syneresis / Aging

After the gelation, the condensation reaction would not stop. It would continue after the gel point causing strengthening and stiffening of the network. Continuous condensation after gelation would cause the gel network to shrink and expel the liquid from the pores. This process is called syneresis. For a wet gel, there are two modes of shrinkage, see Figure 17 [54]. The first kind of shrinkage is produced when the liquid is allowed to evaporate, so the reduction of the volume is with the shrinkage of the wet gel. The second kind of the shrinkage is due to the expulsion of liquid from the gel without any evaporation and this process is called syneresis. Syneresis is the property of many types of gels.

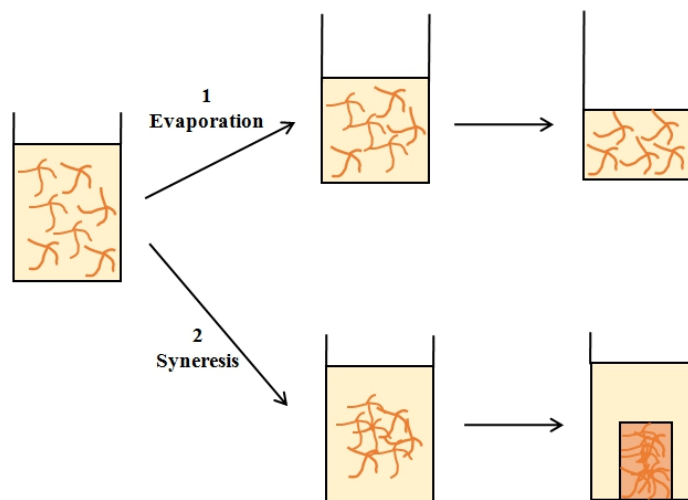


Figure 17 Shrinkage modes for wet gels [54]

2.3.2.5 Drying

The last step in the sol gel process in order to obtain the final ceramic product is

drying of the gel. If the solvent is evaporated in ambient condition, the movement of solvent would make the gel under large capillary forces leading to the collapse of the network, and products obtained after this uncontrolled drying method are called the xerogel. Dense ceramics can be achieved after heating the xerogel. Another drying method should be operated in super critical conditions. The solvent could be extracted and replaced by air under supercritical drying and the resulting products are called the aerogel. Aerogel is arousing more and more interest because of its light weight and excellent properties.

2.3.3 Sensors derived from sol gel technology

As the simple methods for preparing ceramic materials, sol gel technology can be used to manufacture ceramic sensors including optical sensors, mechanical sensors and chemical sensors including gas sensors [55].

Due to the excellent optical properties of the sol gel thin film, compared with optical sensors prepared with other technologies, the sensors based on sol gel technology exhibit better performance. The interaction between the thin film and the light changes because of external factors such as temperature or pressure change and the addition of optical sensitive molecules. Suah et al. [56] combined the optical fiber with sol gel thin film to make a pH sensor with a broad testing range of 2.0 - 12.0 and shorter response time of 15 - 150 s.

Since thin film derived from sol gel technology possess a high flexibility, it is suitable to make a composite from sol gel thin film as a strain sensor. As stated in the

work from Gullapalli et al. [57], a flexible piezoelectric ZnO-paper is synthesized via the sol gel route and it is mixed with cellulose fibers to form a composite via solvothermal method. Its application as a strain sensor is also tested, demonstrating its high sensitivity and linearity at various frequencies.

Sol gel process is also used to synthesize metal oxide nanoparticles for fabricating semiconducting gas sensors as well. Adamyan et al. [58] synthesized tin oxide nanocrystals and tested the sensing performance towards hydrogen gas. The sensor shows a linear response between 50 ppm and 5000 ppm of hydrogen gas at 100 - 130 °C with a short response time of less than 10 s. In [59], tin oxide aerogel is prepared via epoxide-assisted gelation and ambient pressure drying. The resulted aerogel has a highly porous structure and a high sensitivity towards carbon monoxide.

In this thesis, an acetone gas sensor based on tin oxide sol gel is made. The printability and the sensing performance of the sensor is tested.

In the next section, the mechanism of detecting diabetes via breath analysis will be reviewed, including general background of medical diagnosis via human breath and relationship between blood glucose level and breath acetone concentration. Current techniques on human breath analysis will be summarized as well.

2.4 Diabetes detection via breath analysis

2.4.1 Medical diagnosis and human breath

The history of using human breath for the detection of diseases begins with the birth of early medicine. Records in ancient literature show that analyzing the smell of

the breath has been considered as one of the most important methods for medical diagnosis in traditional Chinese medical science for over 3000 years. It is the same with Western medicine. The most famous physician in ancient Greece, Hippocrates, who is referred to as 'the Father of Medicine', proposed that breath information may disclose healthy conditions for human to some extent. Over the past decades, the development of modern medicine and the appearance of more and more related research provide scientific evidence for the validity of this non-invasive diagnostic technique. In addition, the invention and improvement of modern sensing and measuring technologies gradually change the great idea into a precise science which could be used in more accurate applications.

Research work done by Pauling's group in 1971 [60] laid the foundation for modern breath analysis. They developed a gas-liquid partition chromatography system and successfully detected around 250 substances in an exhaled breath sample for the first time. Popov's review article [61] published 40 years after Pauling's research proved that there are more than 3500 different substances existing in human breath including small inorganic molecules (NO, O₂, CO₂, etc.), volatile organic compounds (alcohols, ketones, esters, etc.) and nonvolatile substances (isoprostanes, hydrogen peroxide, leukotrienes, etc.) and this number is continually increasing. Among all these chemically distinct compounds, volatile organic compounds (VOCs) are most commonly used for medical diagnosis due to the fact that breath profile of specific VOCs of patients with particular diseases differs from that of healthy persons. Although there are up to 3000 VOCs which may be detected from human breath, only

very few of them are related to medical diagnosis and monitoring. Table 3 summarizes some common VOCs for detection of diseases.

Table 3 VOCs as biomarkers for disease detection [62][63]

VOCs	Disease
Alkanes, alkane derivatives and benzene derivatives	Lung cancer
Isoprene	Cholesterol metabolism
Acetone	Diabetes mellitus
Sulfur-containing compounds	Liver impairment
Nitrogen-containing compounds	Uremia, kidney impairment
C4-C20 alkanes and monomethylalkanes	Heart transplant rejection
Pentane	Myocardial infarction

Different VOCs have different sources which could be divided into two categories. The first kind of VOCs originates from substances in the external environment entering human body via skin absorption, inhalation and ingestion, which would possibly be metabolized in vivo and excreted through exhaled breath gas. The second kind of VOCs stems from normal physiological activities such as basal metabolism and activity of intestinal bacteria [64]. Breath profile of VOCs could be influenced by many factors including healthy conditions, in vitro environments and sports status, age and gender may have an impact on the concentration of specific VOCs appearing in breath gas as well.

Acetone, as the biomarker for diabetes mellitus, has been researched for several

decades. In the next subsection, details about breath acetone mechanism and the potential of acetone detection for diabetes diagnosis and monitoring would be elaborated.

2.4.2 Breath acetone and blood glucose level

Acetone (C_3H_6O) is a colorless volatile organic component with a characteristic odor. As early as the year 1798, a smell of 'decaying apples' was identified for the first time in the exhaled breath for patients with diabetes mellitus by John Rollo and the special odor was proved to come from breath acetone in 1857 [64]. Along with acetoacetate ($C_4H_6O_3$) and 3- β -hydroxybutyrate ($C_4H_8O_3$), acetone is produced in the liver as well, forming three ketone bodies in human body. Two mechanisms could account for the in vivo formation of acetone, namely, the decarboxylation of acetoacetate and the dehydrogenation of isopropanol [65]. Most of the acetone in human body are produced by oxidation of free fatty acids. Figure 18 elaborates the details of acetone production process via decarboxylation of acetoacetate deriving from fatty acids [66][67]. A small part of blood acetone could diffuse into breath and urine with a fixed ratio (the ratio between breath acetone and plasma acetone is around 1/330 according to [64]) and that's why acetone could be detected in the exhaled breath.

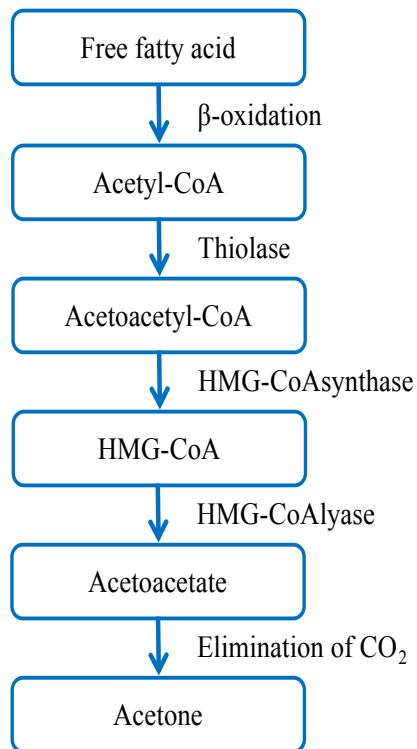


Figure 18 Physiological path of acetone production from fatty acids

Since the major amount of excreted acetone are generated from the oxidation of free fatty acid, breath acetone concentration depends on oxidation level of free fatty acid to some extent. Thus, for patients with untreated diabetes mellitus and uncontrolled insulin level, more fat is broken down in the human body through lypolysis into fatty acids which would finally be converted to carbon dioxide, water and energy, instead of glucose decomposition, as the main energy source. As a result, more ketone bodies are produced as the by-products of using fat to produce energy and higher acetone concentration could be detected in plasma, urine and breath. In other words, things related to facilitating human body to convert fat into energy would increase the acetone level, including diabetic ketoacidosis, physical exercise, fasting and high-fat diets.

According to American Diabetes Association (ADA), diabetes could be divided

into four categories, including type I diabetes with inadequate production of insulin, type II diabetes without proper use of insulin, gestational diabetes and diabetes caused by other reasons. During the past decades, more and more research projects have appeared in order to understand the relationship between breath acetone concentration and blood glucose level to provide basis for diabetes detection via breath analysis. Some positive results have been achieved which confirm the potential significance of research works on development of breath analysis technologies.

The first research trying to find the relationship between breath acetone and diabetes mellitus dates back to 1950s [68]. In 1952, Henderson et al. designed both physical (mass spectrometer) and chemical methods to analyze the concentration of condensed acetone from exhaled breath for both diabetic subjects and normal subjects. Results show that breath acetone concentration for non-fasting subjects is significantly higher than that of nonfasting normal subjects, with the mean value rising from 4.6 μg per gram condensate per unit surface area for normal group to the value of 9.1 μg for diabetic group. Based on their research, there is also a trend that exhaled acetone amount for children is higher than that for older people. In 1960s, research work conducted by Rooth [69] and Tassopoulos [70] are published on *The Lancet* confirmed the increasing trend of breath acetone for patients with diabetes. As the earliest research without too many references, though simple and not so accurate, they did open the prelude to this research area.

From the year when the first research is published, very few articles were published on the topic of breath acetone and diabetes mellitus until the turn of the

century. In 1998, Nelson et al. [71] investigated the exhaled acetone and isoprene for children with type I diabetes mellitus. While there are no significant differences for breath isoprene between diabetic children and healthy children, obvious differences on breath acetone have been observed. In addition to that breath acetone amount for diabetic children are much higher than normal children, an increase of breath acetone level was recorded for diabetic children after fasting for one night without intaking insulin before breakfast and the value keeps growing after the breakfast. Turner et al. [72] monitored breath acetone concentration using selected ion flow tube-mass spectrometry (SIFT-MS) while measuring blood glucose level at the same time during insulin clamp for type I diabetic patients and achieved the relationship that concentration of breath acetone decreases with the decrease of blood glucose concentration.

Similarly, some research on type II diabetes confirmed the effectiveness of diagnosis of diabetes via breath analysis as well. Deng et al [73]. combined gas chromatography-mass spectrometry (GC-MS) and solid-phase microextraction (SPME) to measure the exhaled acetone concentration for 15 type II diabetic patients with comparison of normal subjects and achieved the results that diabetic breath has a mean acetone concentration of larger than 1.71 ppm while the average acetone concentration for normal subjects is 0.76 ppm. Similar trend was achieved by Greiter et al. [74] with type II diabetes using proton transfer reaction-mass spectrometry (PTR-MS) as well.

In the previous statement, detection technologies such as GC-MS, PTR-MS and

SIFT-MS are mentioned. In the next section, current detection technologies including but not limited to the aforementioned ones would be introduced and elaborated in detail.

2.4.3 Current detection technologies

Several techniques have been used in breath analysis including gas chromatography, mass spectroscopy-based techniques, laser spectroscopy-based techniques and gas sensors. Different techniques have different advantages and limits. Details are given in this section.

Gas chromatography (GC) is a method to separate and analyze a mixture of gas. The key component in a gas chromatograph is a column containing a stationary phase similar to the method of column chromatography. The carrier gas, often a stream of inert gas containing the analyte, passes through the column and reacts with the liquid stationary phase coated on the surface of the column, leading to different reaction time for different species in the mixture. Thus, the gas mixture is separated and analyzed based on characteristic elution time of the components called retention time. The column in a gas chromatograph is located in an oven so that the temperature of the gas phase could be changed and controlled. In the detection of VOCs, gas chromatography is always combined with mass spectroscopy, forming a common VOC detection technology called gas chromatography-mass spectroscopy (GC-MS). The gas mixture is separated by gas chromatography according to aforementioned mechanism and analyzed by mass spectroscopy based on different mass-to-charge

ratios of the ions [75].

Another two mass spectroscopy-based techniques commonly used in detection of VOCs are proton transfer reaction mass spectroscopy (PTR-MS) and selected ion flow tube mass spectroscopy (SIFT-MS) [76][77]. The principals for these two techniques are similar. They both use reagent ions to ionize gas components with higher ion affinity, typically VOCs. The difference between these two techniques lies in that the only reagent ion used in PTR-MS is the aqueous cation H_3O^+ , while in SIFT-MS, H_3O^+ , NO^+ and O_2^+ could be used as the precursor ions.

Laser spectroscopy is also a common type of technique used in breath analysis due to its excellent sensing abilities including high sensitivity, high selectivity and rapid response. However, only very few of techniques in this category are applied in detection of breath acetone and cavity ringdown spectroscopy (CRDS) is one of them. CRDS refers to the technique that determines the concentration of the gas species in the gas mixture based on the specific wavelength of the light at which the analyzed gas absorbs. Wang et al. [78] used this approach to monitor relations between breath acetone and blood glucose level and obtained a linear relationship between these two values.

The techniques described above are all efficient detection techniques with high sensitivity and high selectivity and that is why they have already been used in some clinics for breath analysis. However, due to the fact that all these techniques use large and expensive equipment and need professional knowledge for the operation, these techniques are not suitable for daily monitoring and controlling of chronic diseases

such as diabetes at home. In order to create a portable device which is simple for everyone to use, metal oxide semiconducting gas sensors for diabetes monitoring are arousing researchers' interest. Also, with the development of nanotechnology, the sensitivity of the gas sensors is improved dramatically due to the increase of the surface-to-volume ratio. Published research shows that sensors made with metal oxide semiconducting nanoparticles such as WO_3 , SnO_2 , In_2O_3 have great potential on sensing acetone with trace concentration. Section 2.2 presented detailed information about semiconducting gas sensors. In this thesis, a tin oxide sensor is fabricated via aerosol jet printing for acetone detection.

Chapter 3 Preparation and characterization of sensing material

In this chapter, a tin oxide sensing material is selected and prepared. Characterizations have been done on the tin oxide thin film and the sensing performance of the synthesized material has been tested. Details about how to design and build a testing chamber for gas sensors is explained here and influencing factors on repeatability and reproducibility of the sensing response are carefully analyzed.

3.1 Material selection

Among all the semiconducting metal oxide sensor research, tin oxide is one of the most popular materials and it is selected as the sensing material in this thesis since tin oxide is a semiconducting material with a wide band gap of 3.6 eV and it has unique optical and electrical properties. Lots of publications on tin oxide gas sensors demonstrate the advantages of tin oxide compared with other metal oxide materials including its low cost of starting materials and its high sensitivities to target gases. Meanwhile, operating temperature, response and recovery time and selectivity of tin oxide gas sensors are possible to be controlled by modifying surface morphology and adding some dopants [79].

Sol gel technology is chosen as the synthesis method in this thesis due to its low cost, simple operation and the unique film quality obtained from sol gel route. Also, since it is a wet chemical approach and the particle size synthesized from this method is low enough, it is easier to make nanoparticle ink from this technique for the later aerosol jet printing process.

3.2 Material preparation

The aim of the research is to fabricate a gas sensor to detect acetone vapor that could be potentially used for diabetes detection and monitoring via breath analysis. In order to synthesize sensing materials for the desired purpose, tin oxide is selected as the material and sol gel method is used for the synthesis. Thus, meanwhile, another aim of the research is to investigate sol to gel transition process using the example of tin oxide and find the optimal process parameters for making tin oxide sensing

materials.

For preparing the tin oxide sol, 8.4 g $\text{SnCl}_2 \cdot 2\text{H}_2\text{O}$ is dissolved in 100 mL absolute ethanol, as reported in [80]. The mixture is heated to 80 °C and refluxed while stirring. Figure 19 shows the experimental setup. After stirring for 2 hours, the heat source is turned off and the mixture is continuously stirred until it cools down to room temperature. The resulting solution is a stable colloidal solution with light yellow color, as shown in Figure 20.



Figure 19 Experimental setup for synthesizing tin oxide sol

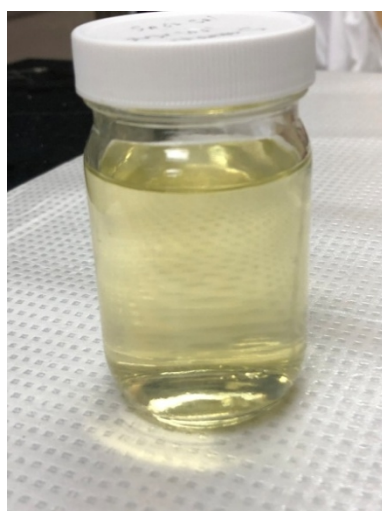


Figure 20 Stable tin oxide sol

All the material characterization work are based on tin oxide thin film coated with the above-mentioned tin oxide sol. Sensing film is fabricated via dip coating technique on a glass slide. For dip coating, a tensile tester with a z-axis motorized stage is used as illustrated in Figure 21. Before coating, the glass substrate is immersed in a container full of ethanol and cleaned by ultrasonic cleaning for 10 min. During dip coating process, the substrate is immersed in the synthesized liquid sol and soaked for 3 min before pulling off from the liquid with the speed of 0.45 mm/min. After each coating, the film is dried in the air before coating for another time. For each substrate, dip coating process is repeated for 5 times in order to have enough sensing material on the substrate. After dip coating and drying in air ambient, the sample is annealed in a muffle furnace at 450 °C for 20 min with the heating rate of 2 °C/min.



Figure 21 Dip coating setup (A tensile tester with z-axis motorized stage)

3.3 Material characterization

3.3.1 Surface morphology (SEM)

In order to investigate the surface morphology of the tin oxide film, scanning electron microscopy (SEM) image is taken via a Tescan Vega 3. As shown in the image, the sensing layer has a smooth surface. To verify that the composition of the thin film is tin oxide, a chemical mapping is conducted with the Energy Dispersive X-Ray Analysis (EDX). Figure 22 shows the SEM image of the layer surface and the distribution of tin and oxide elements on the surface. The chemical mapping proves that tin oxide material is formed on the surface and the distribution of the tin element is uniform.

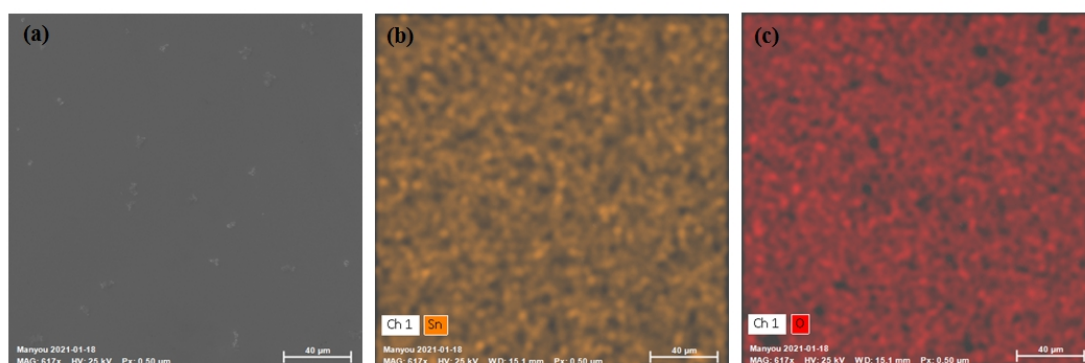


Figure 22 Surface morphology of the sensing layer

(a) SEM image of the smooth surface; (b) chemical mapping of tin element;

(c) chemical mapping of oxygen element

3.3.2 Crystal structure (XRD)

X-ray diffraction (XRD) analysis is conducted with an x-ray diffractometer (PANalytical's X'Pert PRO MRD) in order to study the crystalline structure of the tin

oxide film annealed at 450 °C and the resulted XRD pattern is shown in Figure 23. There are four main peaks in the XRD pattern, with the positions of $2\theta = 26.4299$, 33.5409 , 51.7375 and 65.1500° corresponding to crystal planes of (110), (101), (211) and (112) of tin (IV) oxide tetragonal crystalline phase (cassiterite) (JCPDS 01-070-4177). The average crystal size is calculated with Scherrer equation in Jade software. Calculation shows that tin oxide film annealed at 450 °C has a relatively small average grain size of 15 nm.

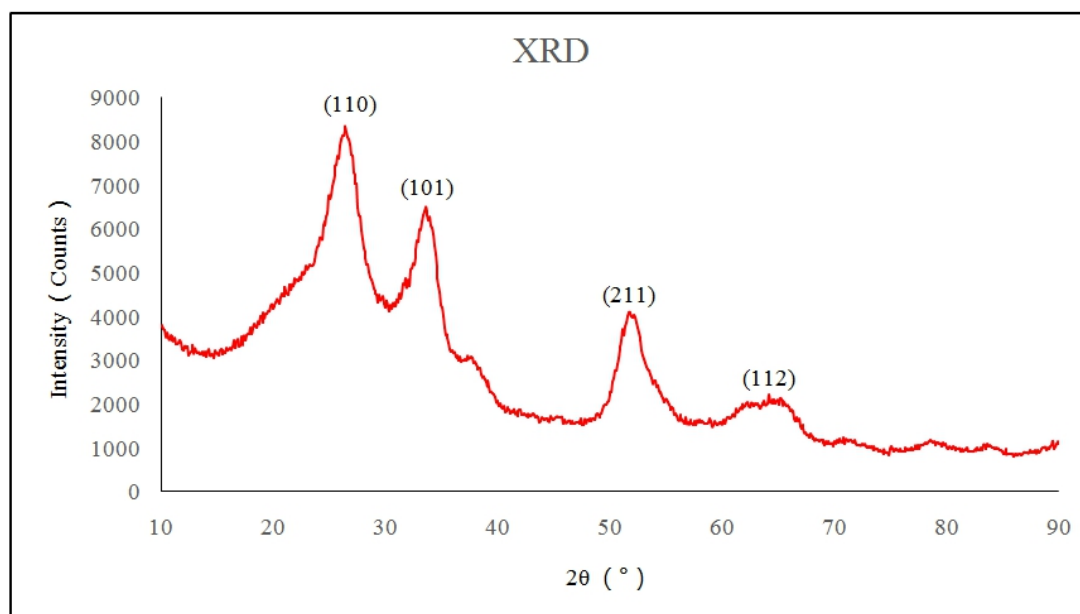


Figure 23 XRD pattern of tin oxide thin film

3.3.3 Optical Properties (UV-Vis)

Transmittance curve (Figure 24) of coated tin oxide thin film is obtained by an ultraviolet-visible light (UV-Vis) spectrometer (Shimadzu UV-2501PC) with a bare glass slide as a reference sample. Since the sample is fabricated via dip coating technique, the transparent thin films are deposited on both sides of the glass substrate.

According to the curve, the transmittance of the material increases rapidly from 300 nm to 400 nm and smoothly transits to a balance up to 900 nm.

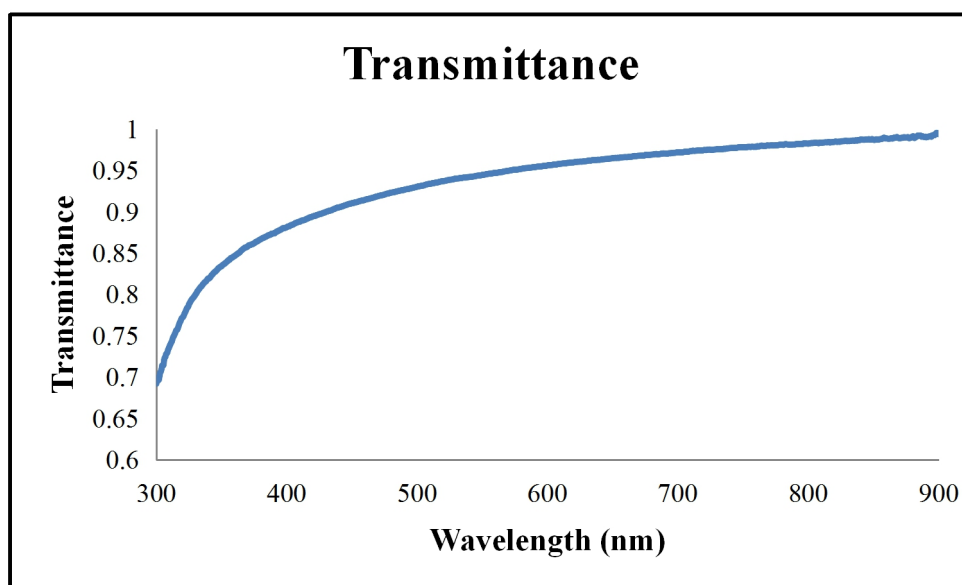


Figure 24 Transmittance of coated tin oxide thin film (after annealing at 450 °C)

3.4 Sol-to-gel transition

Tin oxide sol solution is obtained by dissolving tin chloride precursors in alcohols as mentioned before. After forming tin oxide sol, propylene oxide is added to the solution to initiate gelation. The mechanism is demonstrated in the Figure 25 [74].

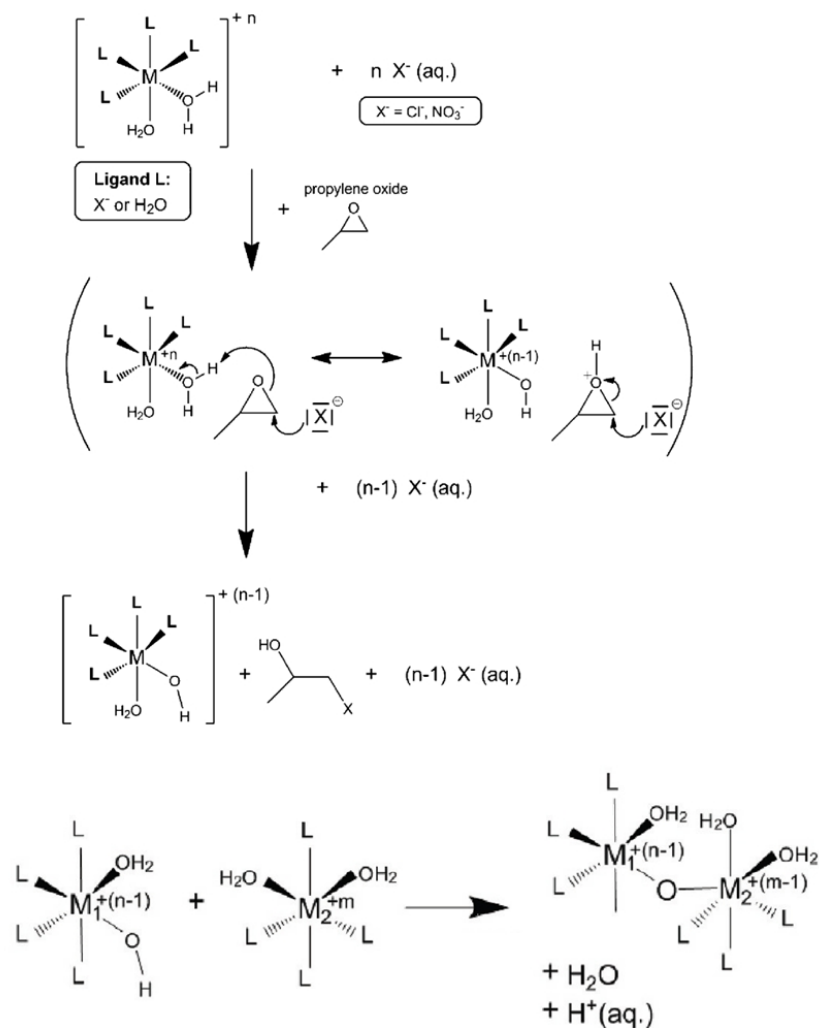


Figure 25 Mechanisms for epoxide-assisted gelation

(Reprinted with permission from [81])

The solution in the Figure 20 is used as the starting sol for gelation. Propylene oxide is added into the solution dropwise while stirring until the liquid completely changes into gel state. After gelation occurs, the material remains stationary when tilting the container. After obtaining the gel material, the container with the gel is put into the Thinky mixer to mix the material for 5 min and put on the hotplate at $50^\circ C$ overnight for aging of the gel. The gel material possesses thixotropy after aging, which means it could become liquid after mechanical shaking and change to gel again

after standing for some time. The resulting material synthesized via this route is yellow opaque gel as shown in Figure 26.

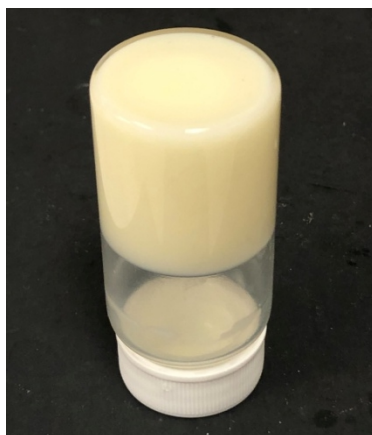


Figure 26 Tin oxide gel prepared from tin oxide sol

3.5 Sensing performance

The sensing performance of the synthesized tin oxide material is tested with the installation of silver electrodes manufactured by aerosol jet printing. The detailed process for fabrication will be elaborated in Chapter 4.

3.5.1 Testing chamber setup

For testing the sensing signals, a home-built testing chamber is made for achieving some specific purposes. A plastic desiccator is selected as the chamber for testing gas sensors. Before setting up the testing chamber, the volume of the selected desiccator is measured by measuring the volume of water that could completely fill the plastic chamber. Figure 27 gives the illustration of the process for measuring the chamber volume. The volume of the chamber is 9.3 L.

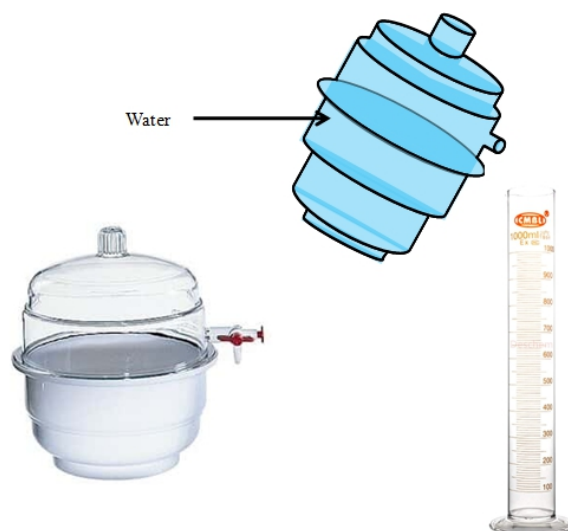


Figure 27 Process for measuring chamber volume

As a testing chamber for VOC sensors, besides the sealed chamber itself, the testing system should also include an inlet for VOCs (acetone in this case), two heaters (aluminum PTC heating plates) -- one for evaporating the solvent and another for elevating the temperature of the sensor in order to achieve the optimal working temperature, a fan (24V DC 3D printer cooling fan) for circulating the air inside the chamber, power supplies (0-30V / 0-10A DC adjustable power supplies) to provide power for the aforementioned equipment and also a sourcemeter (Keithley 2440A) to record the signals of the sensor. In order to achieve the aim, a hole is drilled on top of the chamber for injecting acetone into the chamber. Another two holes are drilled on the side wall of the upper part of the plastic desiccator to make wire connections between equipments inside and outside the chamber. The desiccator is connected to a vacuum pump and an air line as well so that each time after testing, the chamber could be evacuated and fresh air could be purged into the chamber to make sure the chamber before each test is in the air ambient. Figure 28 is the picture of the testing chamber. Figure 29 is a graphic demonstration of the testing system.

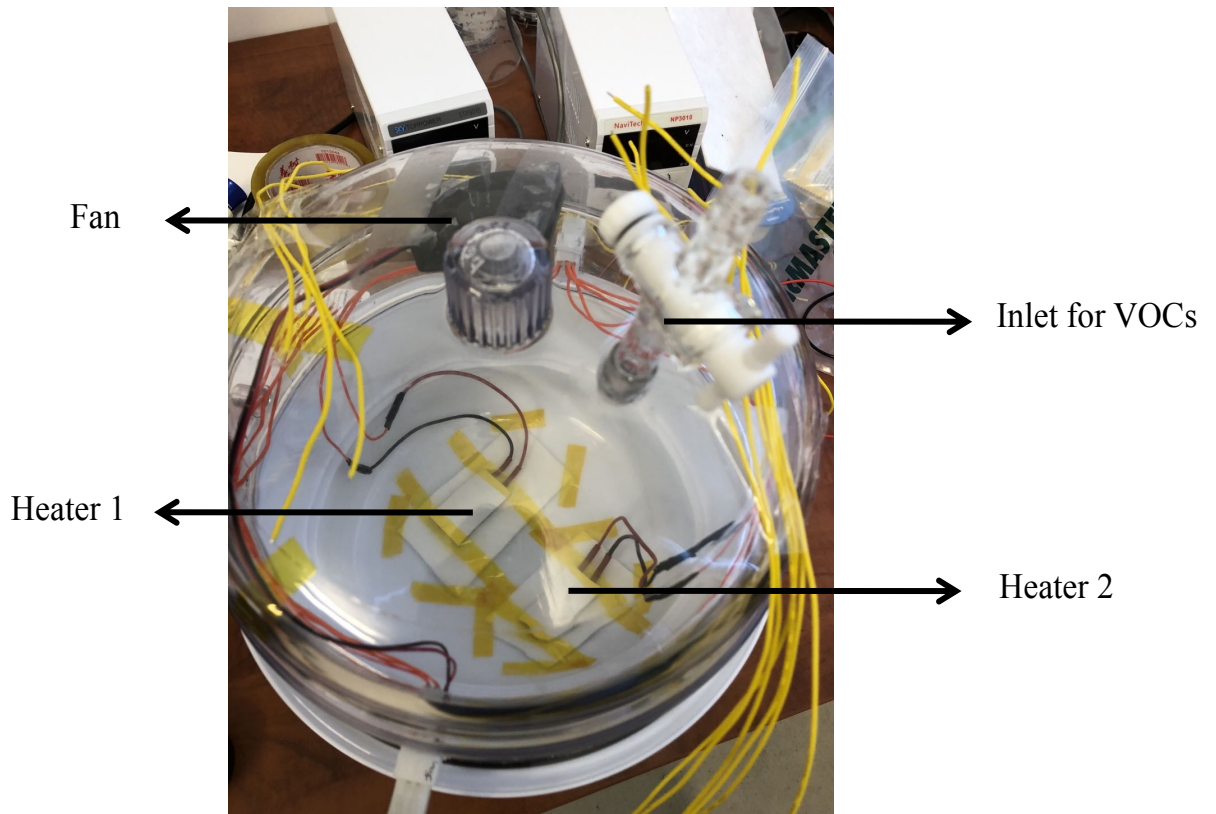


Figure 28 Picture of home-built sensor testing chamber

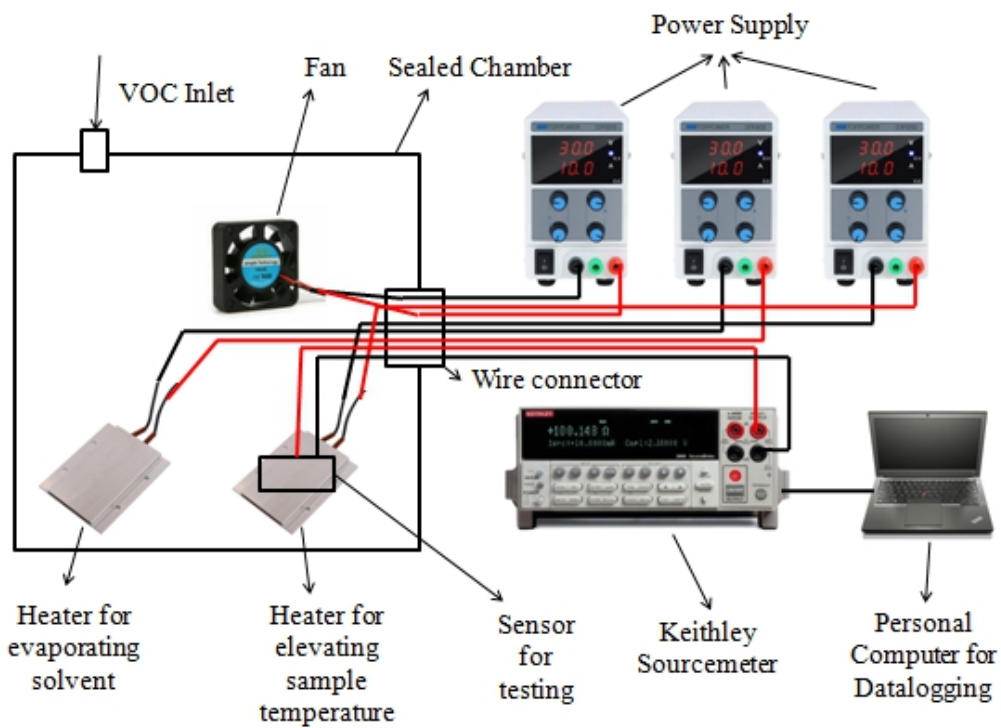


Figure 29 Graphic demonstration of testing system

In order to generate the atmosphere with desired acetone concentration, two

methods have been applied. For acetone environment with higher concentration, liquid acetone droplets are injected into the testing chamber following equation (3.1):

[82]

$$C_{\text{ppm}} = \frac{V_L \times D_L \times T}{M_L \times V_C} \times 8.2 \times 10^4 \quad (3.1)$$

where, C_{ppm} stands for the desired acetone concentration in ppm unit, V_L and V_C represent for the volume of injected liquid (μL) and the volume of testing chamber (mL) respectively, D_L is the density of the liquid (g/mL), T is the testing temperature (K) and M_L stands for the molecular weight of the testing species (g/mol).

For acetone environment with lower concentration, in which case the volume of liquid droplet is lower than the resolution of the smallest syringe and acetone vapor with such a low concentration cannot be created by simply injecting acetone liquid with accurate amount, liquid acetone is injected into a sealed container first to create an environment with high acetone concentration and the acetone vapor is injected into the testing chamber to generate an atmosphere with desired low acetone concentration as described in [83]. Liquid acetone with the volume V_0 (mL) is injected into a sealed container which has a volume of V_1 (mL). After a period of time (~ 30 minutes), acetone vapor is fully evaporated and occupied in the whole container. Under the circumstances, the mole number of the produced acetone vapor is $N_m = D_L V_0 / M_L$, where D_L is the density of acetone liquid (g/mL) and M_L is the molecular weight (g/mol). At the atmosphere pressure P_1 (101325 Pa) and the temperature T_1 (273 K), the resulted acetone vapor has a volume of V_1 ($22.4 \times 10^3 N_m$). At room temperature T_2 (300 K) inside the sealed container, the partial pressure of the acetone vapor (Pa) is

calculated as $P_2 = P_1 V_1 T_2 / T_1 V_2$. The density of acetone vapor ρ_b (g/mL) in the sealed container is calculated as $\rho_b = 10^{-6} \times M_L P_2 / RT_2$, where R is the universal gas constant ($R = 8.314 \text{ kg} \cdot \text{m}^2 \cdot \text{s}^{-2} \cdot \text{mol}^{-1} \cdot \text{K}^{-1}$). When injecting the acetone vapor of volume V_3 into the testing chamber with a volume of V_4 , the concentration of the acetone vapor inside the testing chamber can be calculated using equation (3.2):

$$C_{\text{ppm}} = \left(\frac{\rho_b V_3}{V_4 \rho_{\text{air}}} \right) \times 10^6 \quad (3.2)$$

where ρ_{air} is the air density at room temperature.

3.5.2 Sample preparation for testing

Aerosol jet printed sensor package is used for testing the sensing performance. Detailed fabrication processes of the sensor package will be explained in Chapter 4. Before testing the sensing performance, wires need to be attached on the sensor pad in order to connect the sensor into the electrical circuit. To obtain good adhesion property between the wire and the silver electrode pad, silver paste is used in this project. After applying the silver paste to connect the wire, the whole sensor package, along with the wires, is put in the furnace for a hot cure. The silver paste is cured at $200 \text{ }^\circ\text{C}$ for an hour with a heating rate of $1 \text{ }^\circ\text{C}/\text{min}$ without forming any cracks due to the accumulation of residual stress because of a high heating rate. Figure 30 shows the lead attachment on the pad of electrodes after curing the silver paste.

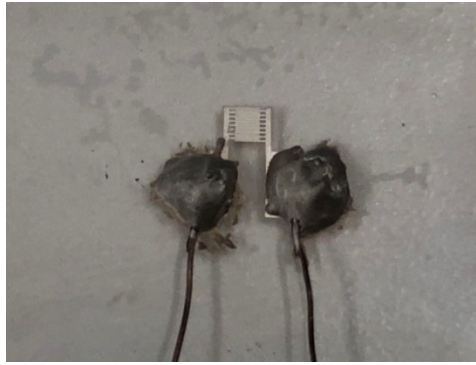


Figure 30 Lead attachment on the sensor pad

3.5.3 Semiconducting behavior and sensing performance

In order to investigate the semiconducting behavior and the sensing performance of the synthesized tin oxide material, three tests have been conducted including current-voltage characterization, resistance change with temperature and dynamic response when exposing to acetone vapor at different concentrations.

3.5.3.1 Current-voltage (I-V) characterization

Figure 31 is the current-voltage curve for the sensing material installed with a pair of electrodes with 50 μm of trace gap. It provides information on the carrier transport behavior from particle to particle or from particle to electrode. The current-voltage relationship is approximately linear, proving that a good ohmic contact is achieved both between the sensing layer and the electrodes and between the electrodes and the wires attached on them. The voltage is increased from 0 to 40 V and then reduced to 0. A hysteresis is observed with the system when the voltage is swept back, a little higher than the original value, suggesting that some carriers are stimulated to the conduction band by applying the voltage.

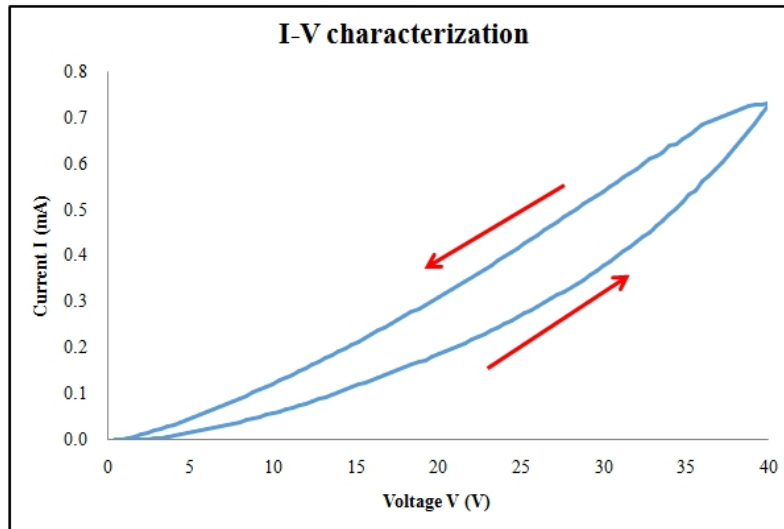


Figure 31 I-V curve for tin oxide sensing layer

3.5.3.2 Resistance change with temperature

Figure 32 explains the charge transport mechanism of tin oxide sensing layer related to temperature. When increasing the temperature, the resistance of the material drops rapidly at first from $G\Omega$ to $M\Omega$ and then gradually decreases to reach a balance. After heating the sensor and cooling it down to room temperature for the first several times, the resistance cannot go back to the original value before heating. The resistance value after a cycle containing heating and cooling is always smaller than the resistance in the previous time. The process should be repeated for more than 5 times in order for the sensor to have a balanced value.

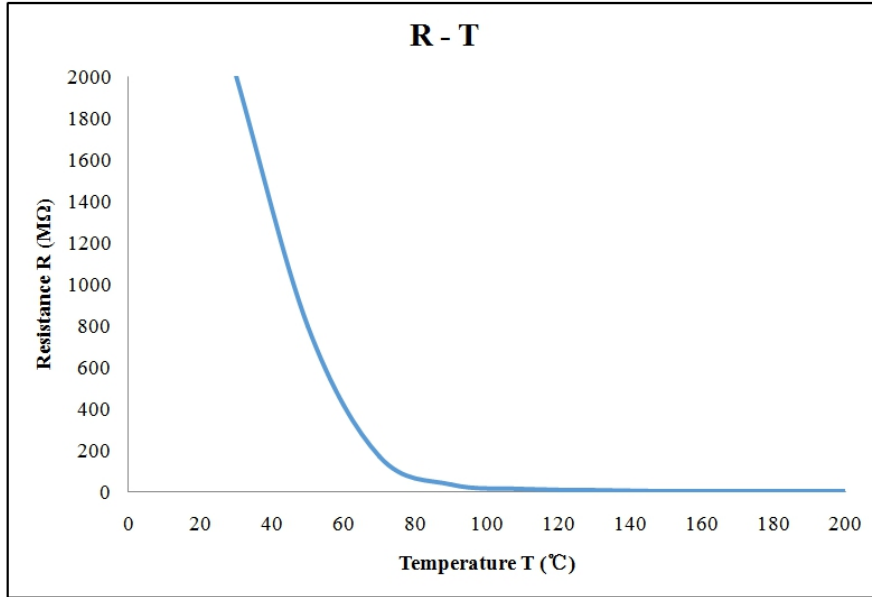


Figure 32 Resistance change with temperature during heating for the first time

3.5.3.3 Dynamic response

Sensing performance of the sensor is tested in the home-built chamber described in section 3.5.1. The temperature used for testing the sensors is 60 °C. Acetone droplets or acetone vapor is injected into the chamber in order to form environments with different acetone concentrations. Real-time resistivity of the sensing layer is recorded and transited to the sensor response. The sensor response is calculated by the following equation:

$$S = \left(\frac{R_a}{R_g} - 1 \right) \times 100\%$$

where R_a is the resistance of the sensing layer in the air atmosphere and R_g is the resistance of the sensing layer when exposing to acetone vapor.

Figure 33 is the dynamic response curve for sensor testing. When the acetone vapor is injected into the testing chamber, the resistance of the sensing layer starts

decreasing until it reaches its lowest value. Then air is purged into the chamber, and the resistance of the sensing layer increases to the original value. Figure 34 shows the linear relationship between the sensor response and the acetone concentration as well.

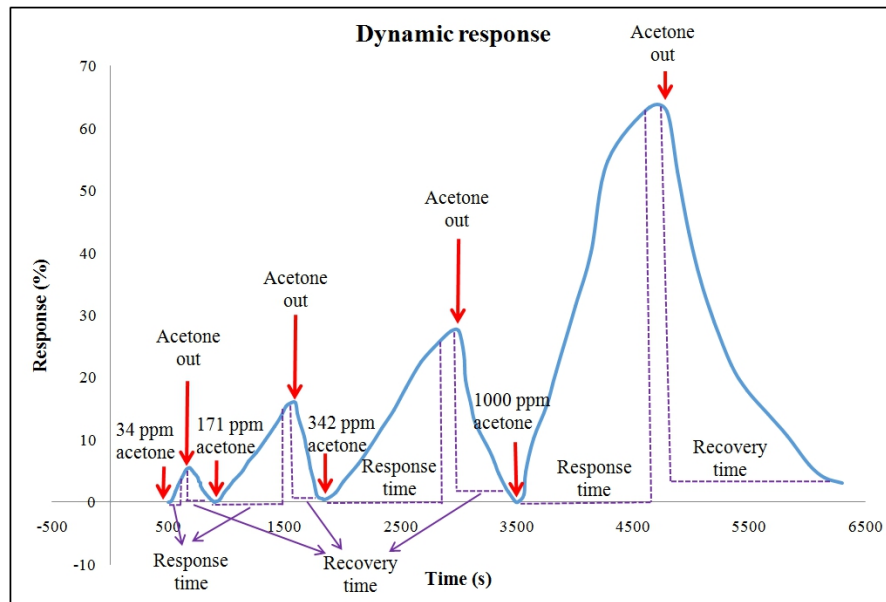


Figure 33 Dynamic response curve for printed acetone sensor

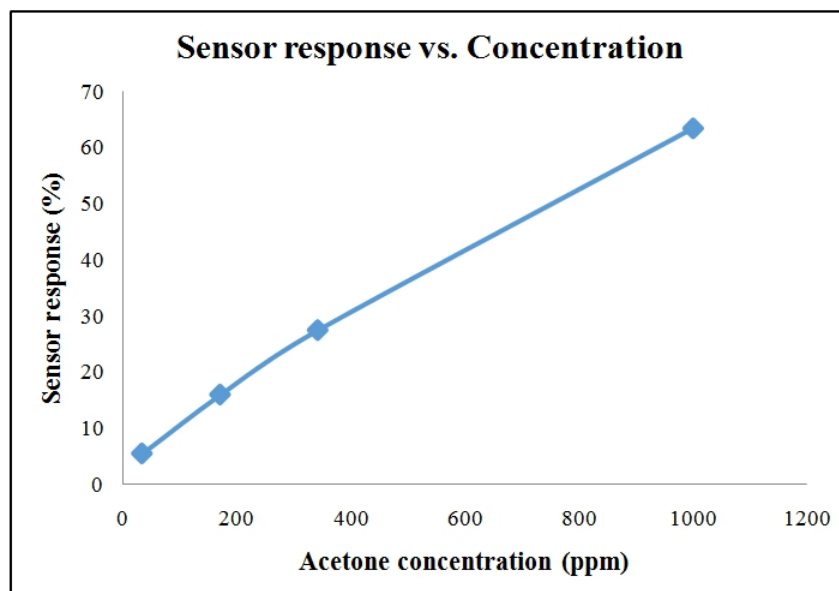


Figure 34 Linear relationship between sensor response and acetone concentration

Another two important factors for a gas sensor are its response time and recovery

time. Response time is defined as the time the sensor reaches the maximum signal when exposing to targeted gas. The time for the sensor resistivity to drop from the maximum value to the original point is called recovery time. Both response time and recovery time are determined based on the dynamic response curve (see Figure 33). In this study, the time to achieve 95% of the sensor response and the time for the sensor to get back to 95% of its original resistance are calculated as the response time and the recovery time. In the testing concentration range, the recovery time increases proportionally with the increase of the acetone concentration. For the response time, it increases rapidly at the concentration lower than 300 ppm and then it steadily grows at higher concentration. As a result, at lower concentrations, recovery time is always shorter than response time, while with the increase of the vapor concentration, recovery time will eventually exceed response time due to a large amount of adsorption.

3.5.3.4 Influencing factors on repeatability and reproducibility

In order to study the repeatability of the manufacturing process, various samples are made following the same fabrication procedure, two of which with linear response towards increasing acetone concentration are selected and compared in Figure 35.

Results show that for both sensors, a linear relationship between sensor response and acetone concentration exists, but the detection range is different between two samples. Sample 1 has linear resistance change from 30 ppm to 1000 ppm. Below this testing range, the sensor could not test any signals and above this range, the response

is not linear to acetone concentration. While for sample 2, the sensor response is approximately linear between 400 ppm and 1500 ppm. Various factors both in manufacturing and testing process may cause visible differences on sensor sensitivity and detection limit.

In the manufacturing process, since the ink is made from tin oxide sol, some characteristics in sol gel chemistry may have impacts on the property of sensing material. Once metal alkoxides or metal chlorides are dissolved in the alcohol, precursor molecules form and percolation process begins, leading to the expansion of the solid skeleton and the growth of the solid particles. Therefore, particle size in the colloidal dispersion keeps changing which may influence the final grain size in the sensing film when printing with the ink made from tin oxide sol with different preservation time. In addition, in the aerosol jet printing process, the liquid amount in the ink vial keeps decreasing with the proceeding of the printing process. Also, the temperature of the water bath and the liquid ink slightly increases when the ultrasonic atomizer is turned on for long time although the printing system is connected to a water chiller for making the temperature of the ink balanced. For aerosol jet printing, a little change in the ink volume or temperature will cause significant change on the printing quality of the printed parts and this change may affect the sensing performance of the printed sensors.

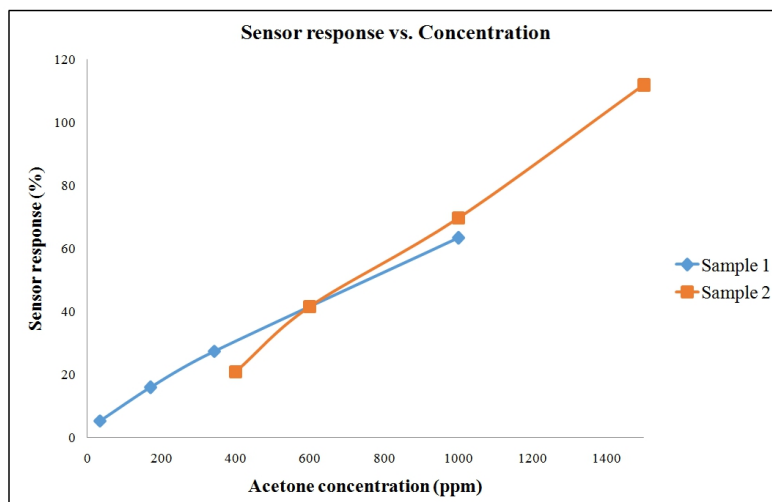


Figure 35 Comparison of sensor response for replicating samples

In the sensor testing process, many factors have influences on the results as well. As described in Section 3.5.1, the sensing chamber is designed and built in lab with common lab supplies, and desired acetone atmosphere is created by manually inject acetone droplets or acetone vapor, so the sensing response achieved in the testing chamber may not be so accurate compared with professional testing systems specially designed for gas sensor research. Before testing, wires need to be attached on the pad of electrodes, the amount of the paste, the length of the wires, the way for connecting the sourcemeter probe to the wire and the voltage applied to the semiconductor during testing are all influence factors for the achieved sensing performance. Additionally, environmental conditions are also important for testing semiconducting sensors. The sensing performance is a function of the temperature and humidity during sensor testing. The temperature of the sensor is controlled by a heater in this project. But environmental humidity is different every time when testing. Thus, samples show different sensing performances at different testing occasions, as shown in Figure 36.

In Figure 36, the same sample is exposed to the same concentration (600 ppm) of acetone vapor and real time sensor response is recorded. The response value of the sensor in two tests are similar but the response time and the recovery time of the sensor differ. Although the results show the reproducibility of the sensor to some extent, the adsorption and desorption mechanism need to be better understood in order to better control the sensor parameters.

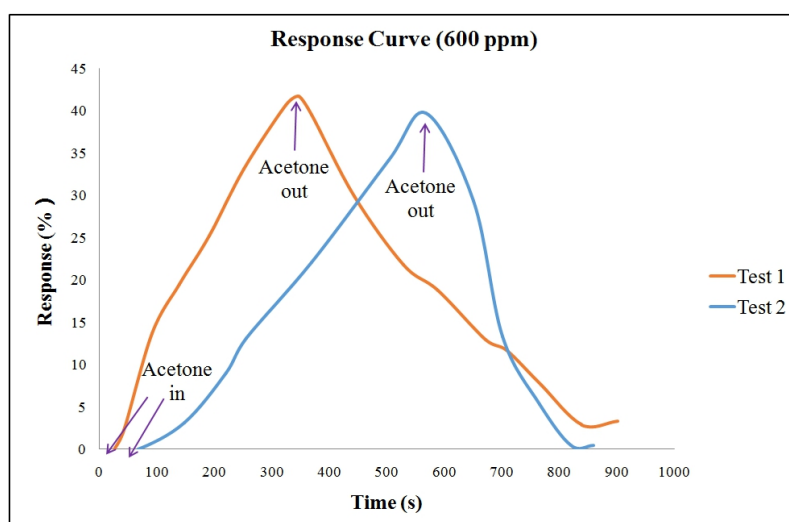


Figure 36 Comparison of sensor response for the same sample

3.6 Summary

In this chapter, the sensing material is prepared via a sol gel route. The material is coated on the glass substrate and annealed for achieving the desired conductivity. The resulted film is used for the characterization of the material including the surface morphology, the crystalline structure and the optical property. Characterization results show that a uniform layer of tin oxide with high transparency has formed on the surface of the glass substrate.

For testing the sensing performance, a testing chamber is designed and built including the heater for elevating the sensor temperature, a heater for evaporating the solvent and a fan for circulating the air inside the chamber. A Keithley sourcemeter is connected to the testing system to record the real time response from the sensor.

For understanding the semiconducting behavior and the sensing performance of the sensing material, current-voltage (I-V) curve, resistance-temperature (R-T) curve and dynamic response curve are obtained. I-V curve shows good contacts among particles and between particles and electrodes. R-T curve demonstrates the semiconducting behavior of the sensing material -- the resistance keeps decreasing when elevating the temperature. The dynamic response curve illustrates the sensing performance of the current material. It has linear response when exposing to acetone vapor under different concentrations. However, the response time and recovery time of the material is long compared with other research.

In the next chapter, detailed processes on how to fabricate a gas sensor package via aerosol jet printing will be elaborated.

Chapter 4 Aerosol jet printing of the gas sensor package

In this chapter, detailed procedures on fabricating gas sensors via aerosol jet printing are elaborated. The printing system used in the thesis and the printing parameters which are important for printing quality are introduced. The printing process is detailed and the printed parts are characterized by optical profilometer images including electrodes, micro-hotplates and the sensing material.

4.1 Printing system

The printer used in this project is an Optomec M³D aerosol jet system. Figure 37 is the image of the printer structure.

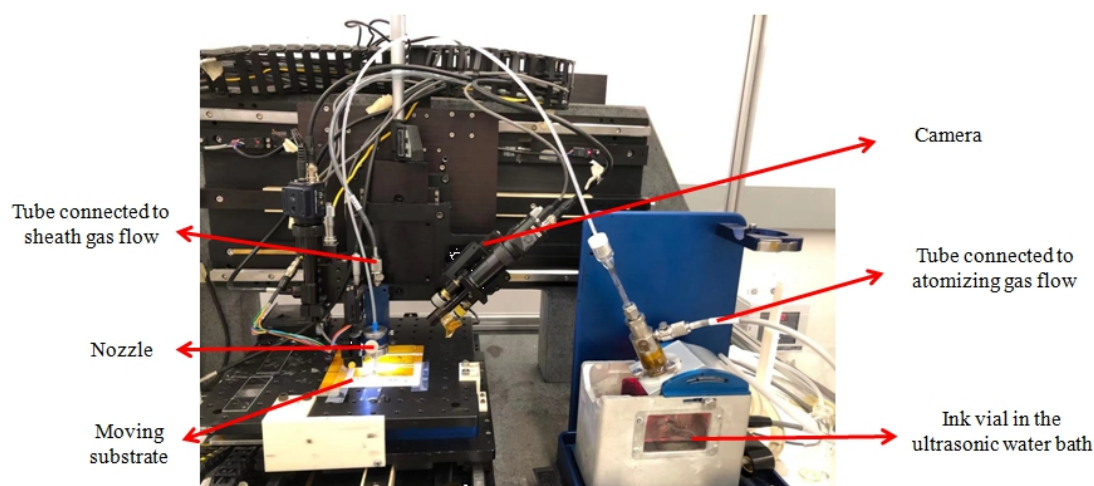


Figure 37 Optomec M³D structure

As shown in the schematic for the printing system, ultrasonic atomization is used as the aerosol generation technique for Optomec M³D aerosol jet printer. Before printing, an ink vial with 1 to 2 mL of ink should be immersed in the ultrasonic water bath. In order to remove the heat generated in the ultrasonic process and keep the temperature of the ultrasonic water bath constant, the water bath is connected to a water chiller usually set to 12 - 20 °C. In order to provide atomizer gas and sheath gas, a nitrogen gas tank is connected to the Optomec system. The tube for atomizer gas flow is connected to the ink vial in order to increase the pressure inside the vial and bring the aerosol gas out, while the tube for sheath gas flow is connected to the back of the nozzle so that the sheath gas could enclose the atomizer gas to form a protective layer to the nozzle wall.

A camera is connected to the Optomec system as well and the real time image

during printing is transited to the computer included in the printing system. During printing, line morphology could be seen on the computer so that printing parameters could be changed and optimized before and during each print. Before executing each print, the height of the nozzle should be adjusted to make the nozzle focused, which could be verified from the real-time camera image on the computer screen. During printing, the substrate table could move back and forward and the nozzle could move left and right, thus, the printer could execute any designed CAD files.

4.2 Process flow

In order to fabricate a gas sensor via aerosol jet printing, several steps should be followed. Since a gas sensor package is consisted of the sensing material, metal electrodes and a micro-hotplate on the backside of the substrate, nanoparticle ink for printing all those parts should be formulated at first. In order for the ink to be printable, trial and error is required. Once the ink is printable, it can be loaded into the printing system to do the test printing in order to find the best printing parameters for each kind of ink. By adjusting printing parameters, line morphology on the computer screen keeps changing. This process should be repeated until the best line morphology (continuous line and no overspray) is achieved.

After obtaining the printing parameters for the ink, the printing file with the designed pattern can be executed. The 2D file can be made with AutoCAD and the CAD file can be transferred to the printing path that the Optomec system could recognize. During printing, Optomec would follow the orders when lines were created

in the CAD file.

After printing, the part should undergo some post treatment processes. For printed metal electrodes and micro-hotplates, the part is sintered at 300 °C in air atmosphere. For printed sensing materials, the film is annealed at 450 °C. Both heat treatments are done in the muffle furnace.

Once the printed part is obtained, microscope images of the part should be achieved in order to find any defect on line morphologies and measure the surface roughness of the part, which would be useful for the future improvement of printing process.

Figure 38 summarizes the process flow for fabricating a gas sensor via aerosol jet printing.

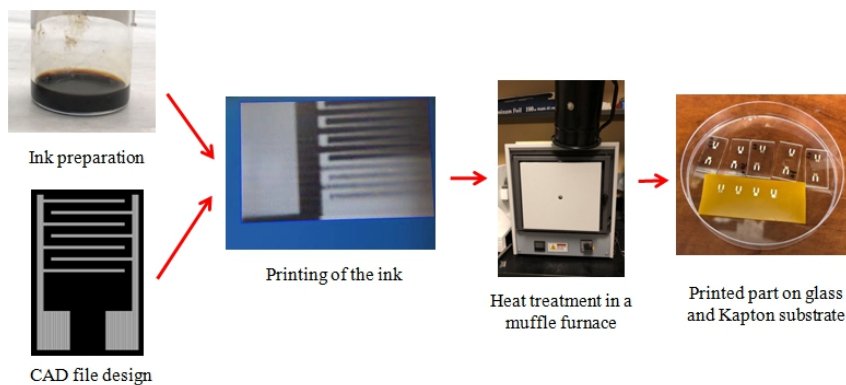


Figure 38 Process flow for printing a gas sensor

4.3 Ink formulation

Two types of ink are used in this project, tin oxide ink made from tin oxide sol as described in Chapter 3 for printing the sensing material and commercial silver nanoparticle ink for printing conductive metal electrodes and micro-hotplates.

For printing sensing materials, tin oxide sol is used as the basis to make the ink. Since the original solvent for tin oxide sol is ethanol and it has a viscosity of 1.095 cP. The sol without any modification is not suitable for generating aerosol in the ultrasonic bath. In order to improve the printability of tin oxide sol, it is mixed with α -terpinol, who has a viscosity of 67 cP, to increase the liquid viscosity of the ink. The volume ratio between tin oxide sol and α -terpinol is 8:2. A total volume of 2 mL of ink - a mixture of 1.6 mL tin oxide sol and 0.4 mL of α -terpinol is put into the vial and used for the printing process. Figure 39 is the picture of the tin oxide ink.



Figure 39 Picture of tin oxide ink made from tin oxide sol

For printing electrodes and micro-hotplates, silver nanoparticle ink is used due to its high conductivity after sintering. The silver ink used in this project is a commercial ink from NovaCentrix. Different vendors for silver ink were compared and NovaCentrix was selected in a previous project. For achieving the best printing performance, the ink is diluted with deionized water with a volume ratio of 1:1. A total amount of 2 mL of ink, with a mixture of 1 mL of silver ink and 1 mL of deionized water, is put into a vial and the vial is placed in a sonicator for 10 min to

make silver nanoparticles disperse better. After sonicating the vial containing the ink, the vial is loaded in the ultrasonic water bath in the Optomec printing system.

4.4 Important printing parameters

Four parameters are important during printing process, namely, atomizer power (Unit: V), atomizer gas flowrate (Unit: cc/min), sheath gas flowrate (Unit: cc/min) and printing speed (Unit: mm/sec). Details of each printing parameter will be followed.

Atomizer power controls the voltage level that is applied to the ultrasonic atomizer. The larger the atomizer power is, the more aerosol will be generated in the ink vial. If the atomizer power is too high, chances are that the nozzle will get clogging more easily because of too much aerosol. Typically, for inks with higher viscosity, a high value of atomizer power should be used for successfully generating microdroplets. With the largest value being 50 V, commonly this value is set between 35 V and 45 V.

Once the atomizer power is selected and a good mist forms in the ultrasonic water bath, another three printing parameters that need to be changed in the printing system are atomizer gas flowrate, sheath gas flowrate and printing speed. In order to study the effects of abovementioned three printing parameters on printing quality, multiple silver lines are printed by changing one of the printing parameters and keeping the other two as constants. During printing, atomizer power is fixed at 40 V. Each silver line shown in the following images is the addition of three times printing

in order to make the line clearer and easier to be analyzed. After printing, images and profiles of the lines are obtained with an optical profilometer.

Atomizer gas flowrate adjusts the amount of atomizer gas flow which brings the aerosol out of the ink vial and transport it to the nozzle for deposition. How to set this parameter should depend on the aerosol amount in the ink vial. If a large amount of aerosol is formed in the vial, a less value of atomizer gas flowrate should be set. If the aerosol amount in the ink vial is not large enough, then the atomizer gas flowrate should be set as a large value in order to bring as much aerosol out as possible from the vial. With increasing the atomizer gas flowrate, the width of the printed line increases. The edge quality of the line improves at first and then deteriorates, as shown in Figure 40. Atomizer gas flowrate could be adjusted from 0 to 50 cc/min.

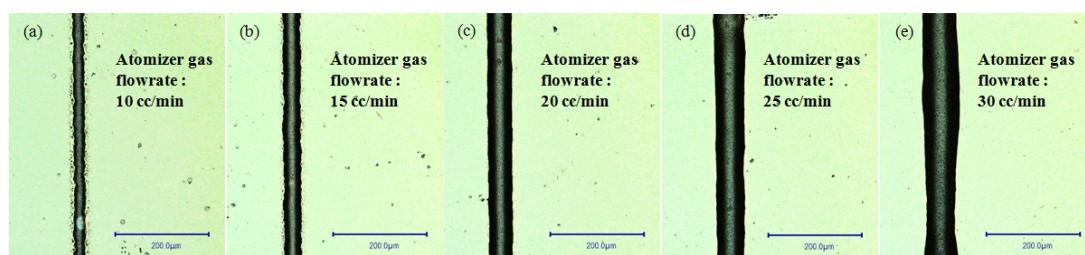


Figure 40 Effects of atomizer gas flowrate on printed line morphology with fixed sheath gas flowrate at 30 cc/min and printing speed at 1 mm/sec

Sheath gas flowrate controls the amount of sheath gas that surrounds the atomizer gas in the nozzle. By changing the ratio between sheath gas flowrate and atomizer gas flowrate, the aerosol jet geometry could be controlled. If the sheath gas flowrate is increased, the aerosol gas stream will be more compressed, so that the printed line will be more focused. However, for some inks, increasing the sheath gas flowrate may also cause overspray, an excess deposition of material out of printed line,

due to the high inertia of the gas stream. In order to make the printed line focused and minimize the overspray phenomenon, a balance should be reached and that is one of the challenges in manufacturing process. Figure 41 shows the impact of changing sheath gas flowrate on line morphology. Sheath gas flowrate could be adjusted from 0 to 200 cc/min.

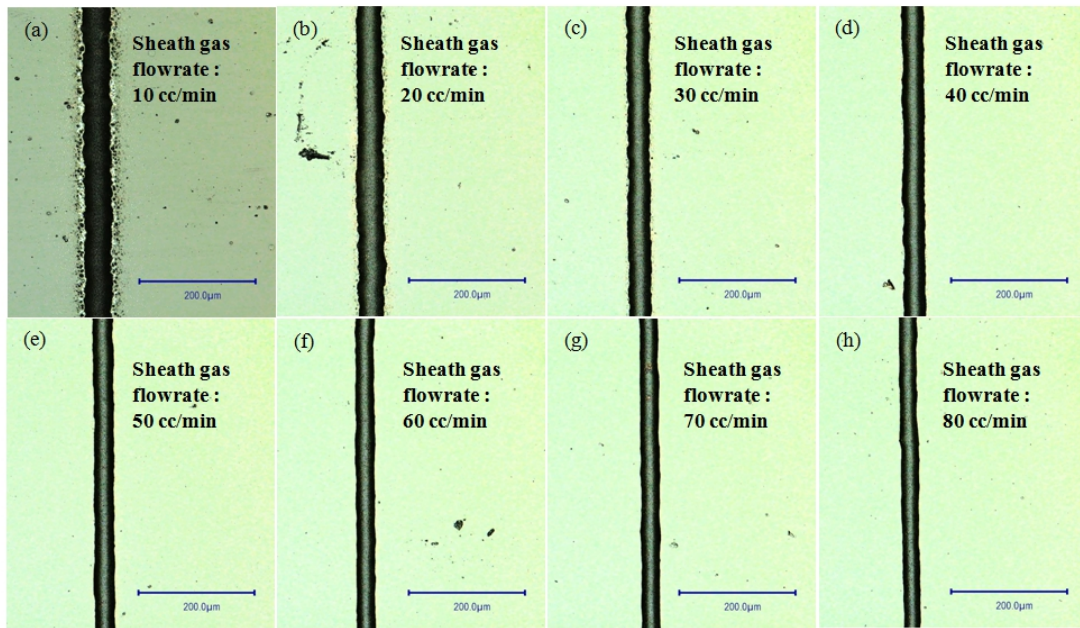


Figure 41 Effects of sheath gas flowrate on printed line morphology with fixed atomizer gas flowrate at 15 cc/min and printing speed at 1 mm/sec

Another factor that would influence the printed line morphology is printing speed. Printing speed controls how fast the printer would execute each line in the designed file. High printing speed could reduce fabrication time, but it will also lead to rough line edges and make the line thinner and even discontinuous, as shown in Figure 42.

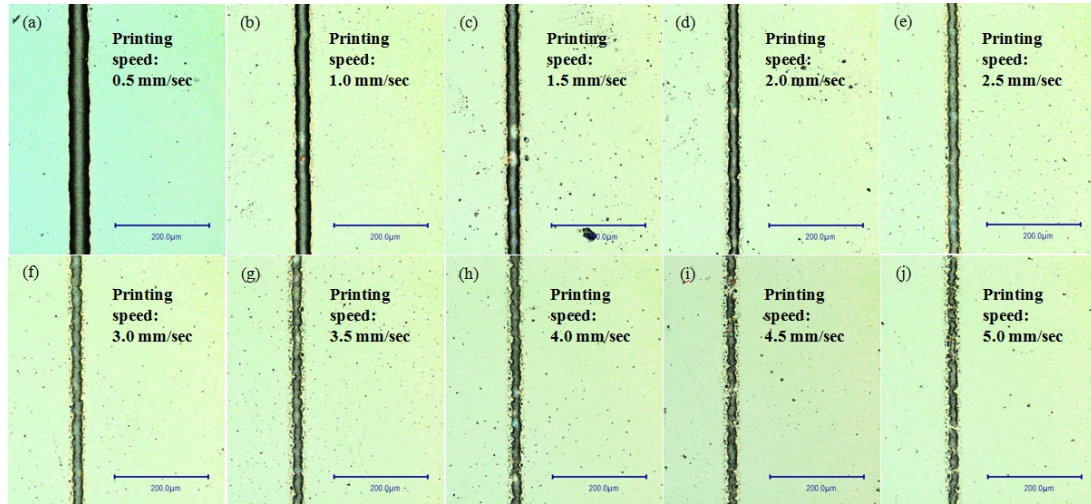


Figure 42 Effects of printing speed on printed line morphology with fixed atomizer gas flowrate at 15 cc/min and sheath gas flow rate at 30cc/min

Figure 43 shows that relationship between printed line width and three printing parameters described above. With the increase of atomizer gas flowrate, the line width keeps increasing, while the opposite trend exists when increasing sheath gas flowrate and printing speed.

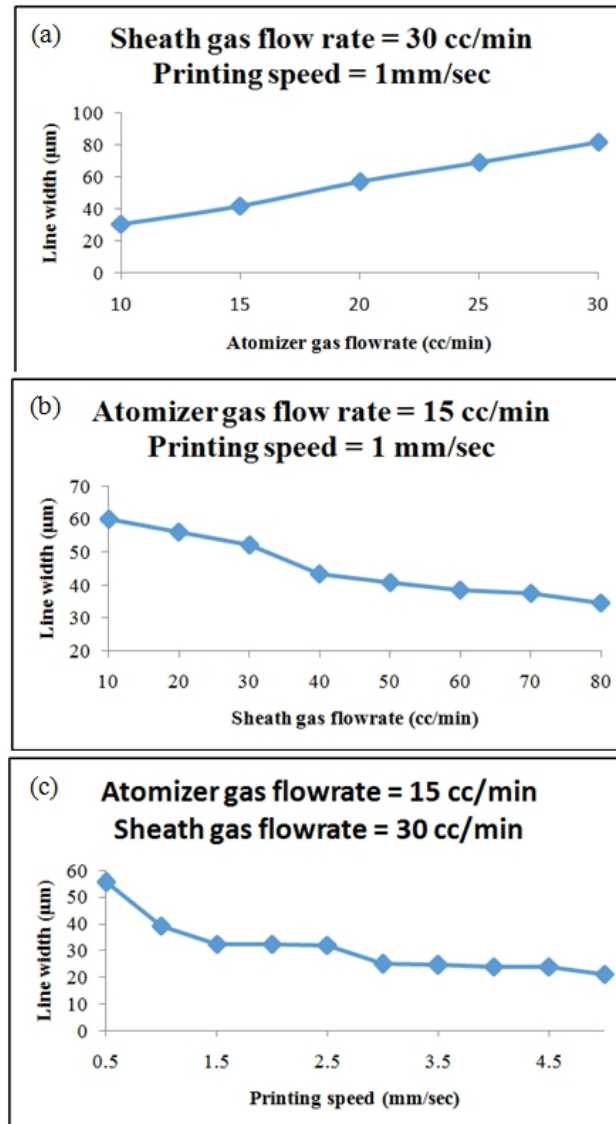


Figure 43 Relationship between line width and printing parameters

4.5 Post treatment process

After having the printed parts, they should be put into the furnace for heat treatment.

For silver electrodes and micro-hotplates, sintering of silver nanoparticles is required in order to convert the compacted silver nanoparticles into an integrated solid body to achieve the desired conductivity. The sintering temperature used in this

project is 300 °C with a low increasing rate of 1 °C/min. After staying at 300 °C for 1 hour, the part is cooling down with the furnace to room temperature.

For tin oxide sensing material, the printed thin film should be annealed in order to increase the ductility, reduce the hardness and form the crystalline structure. The annealing temperature used for tin oxide sensing material is 450 °C in this project. The part is heated to 450 °C with a heating rate of 2 °C/min, then it stays at 450 °C for 20 min and finally cools down to room temperature with the furnace.

4.6 Characterization of printed parts

4.6.1 Electrodes

The advantage of aerosol jet printing on manufacturing electrodes lies in its flexibility to design and print different patterns. Once a CAD file is created, it can be transited to computer orders and the printing process could be executed. For semiconducting gas sensors, gaps between traces are important for the sensitivity. The smaller the gap is, the higher the sensitivity will be. In order to show the flexibility of printing and to minimize the gaps between different trace lines, different patterns are made with AutoCAD and electrodes with different geometries are printed. Figure 44 shows electrodes with different trace gaps (200 μm, 100μm, 50μm and 30μm) before sintering and after sintering.

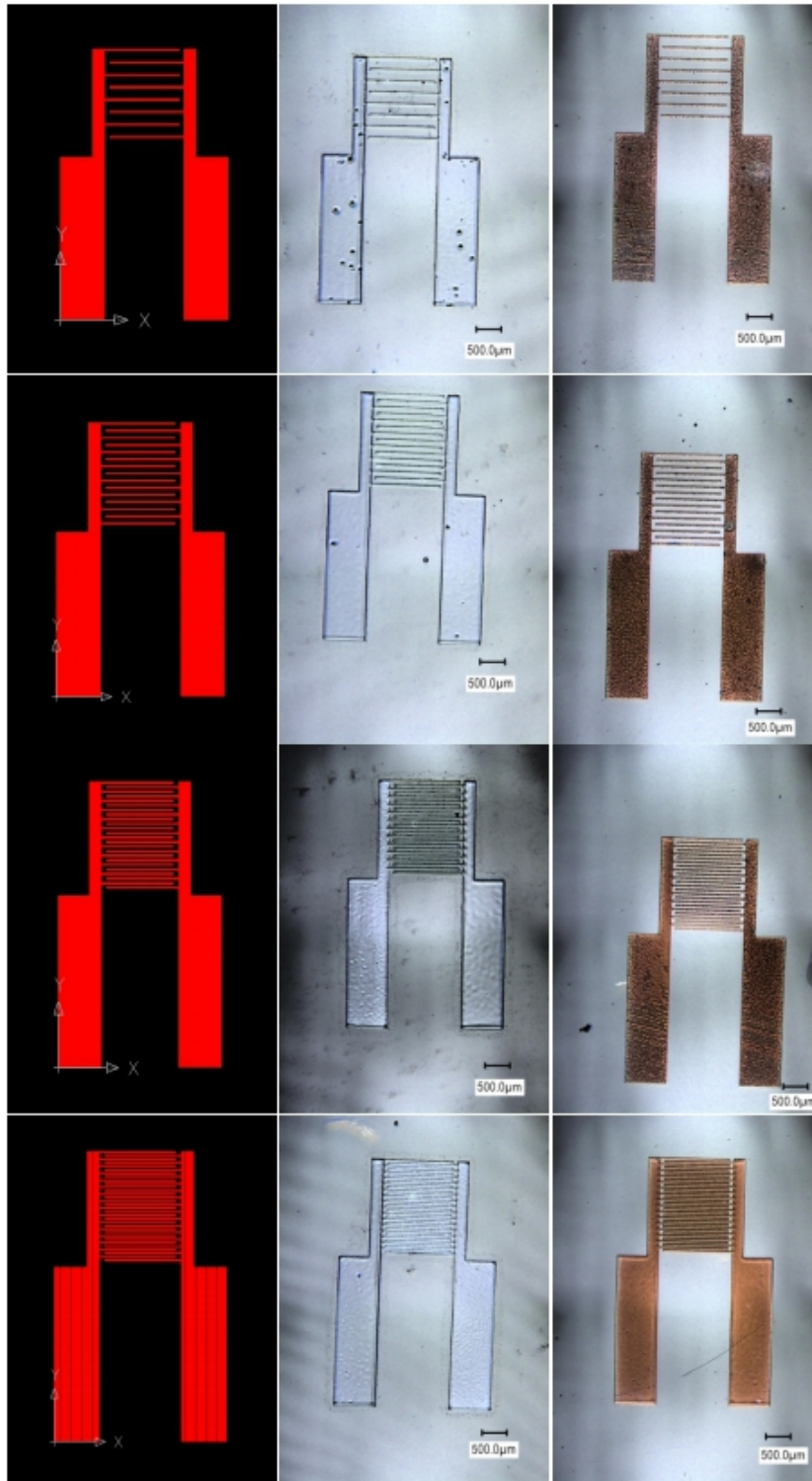


Figure 44 CAD pattern and optical images of electrodes with different trace gaps

Profiles of conductive traces on the electrodes are also measured. Due to the printed line width, the measured distances between conductive traces are smaller than

the gaps designed in the CAD file. For 200 μm trace gap on the CAD file, the measured distance between traces is 177.35 μm for printed electrodes. Similarly, the gap distance of 76.46 μm and 39.12 μm are measured for patterns with 100 μm and 50 μm gap. Also, for a single trace, the thickness is around 2 μm after sintering and the width of the trace is around 50 μm . Figure 45 shows optical images of conductive traces on the electrodes and their corresponding surface profile with trace gaps, line thickness and line width.

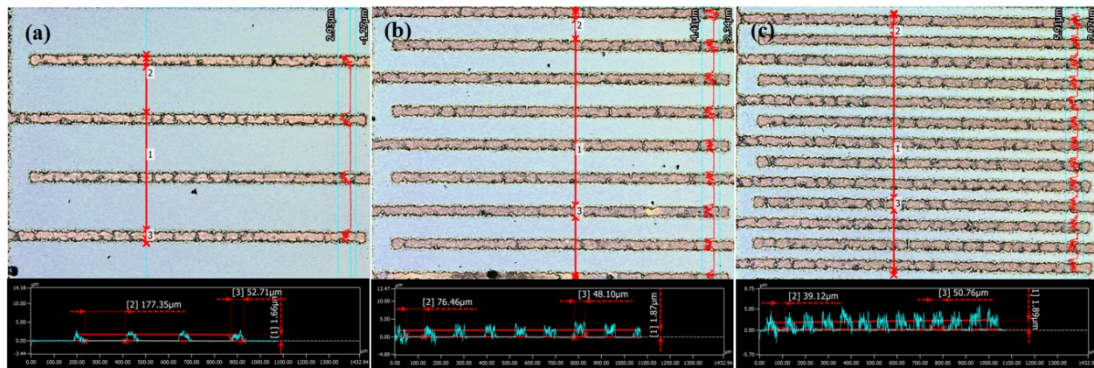


Figure 45 Optical images and surface profile of the conductive traces

When designed gap between traces is 30 μm , traces tend to connect with each other as shown in Figure 46. Meanwhile, there are not any obvious differences with printed traces and bare substrates on the profile image. In this case, when placing two probes on the two pads of the electrodes, the electrical circuit will be shorted and the electrodes lost all the functions.

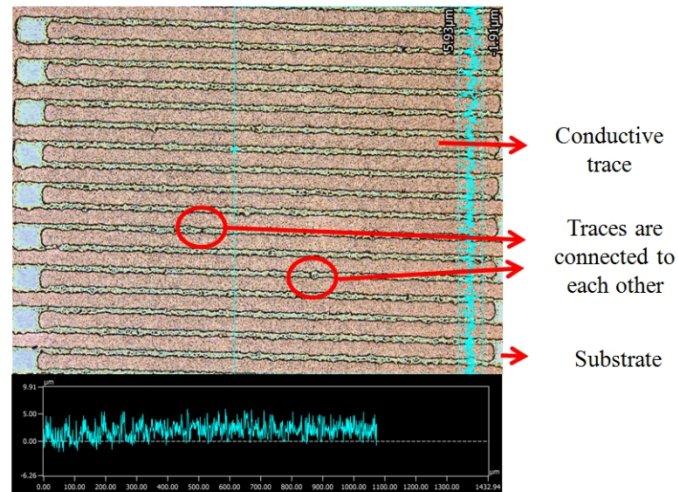


Figure 46 Connected traces under small designed trace gaps

Surface roughness of printed silver electrodes after sintering is measure on the pad area. A smooth surface with a roughness of $0.20 \mu\text{m} \pm 0.01 \mu\text{m}$ is achieved. Figure 47 is the surface image of the electrode pad that is used to measure the surface roughness. The magnification of the optical profilometer used here is 20x.

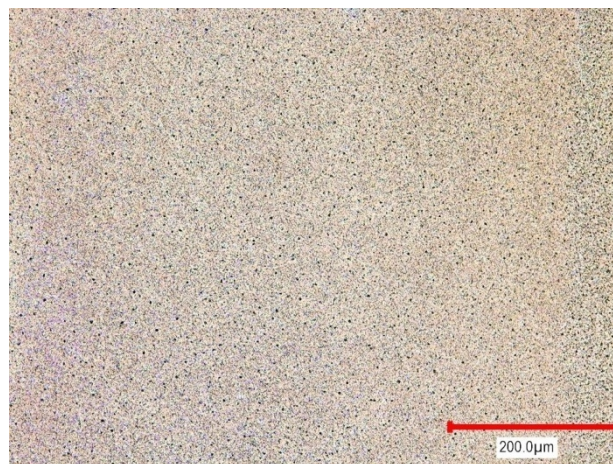


Figure 47 A smooth silver surface with a roughness of $0.20 \mu\text{m} \pm 0.01 \mu\text{m}$

Sintering of the electrodes has been tried both on the hotplate and in the furnace. When sintering on the hotplate, the increasing rate of the temperature could not be controlled, resulting in cracks and defects on the surface. However, this problem

could be solved by controlling the sintering profile in a furnace. Figure 48 shows the differences between uncontrolled sintering on the hotplate and controlled sintering in the muffle furnace.

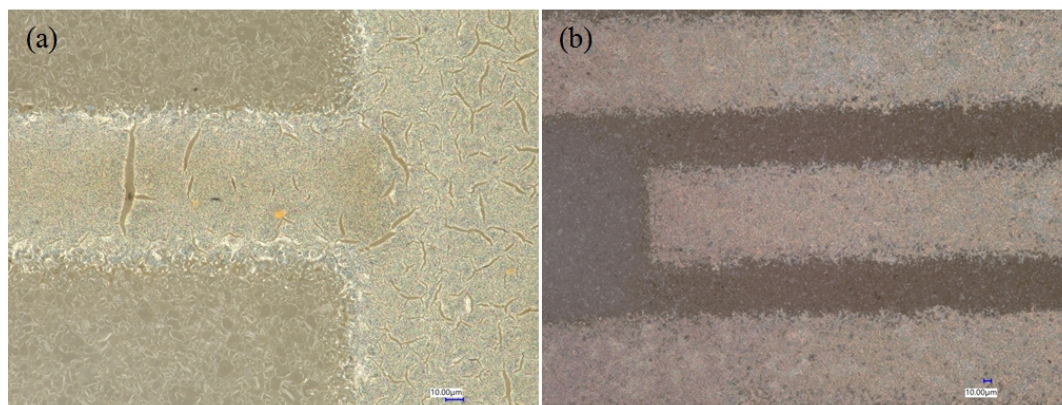


Figure 48 Differences between uncontrolled sintering and controlled sintering
(a) cracks when sintering on the hotplate; (b) continuous path without defects when sintering in the muffle furnace

4.6.2 Micro-hotplates

In the preliminary design of the sensor package, a micro-hotplate should be fabricated on the backside of the substrate to elevate the temperature of the sensing system. Pattern design and aerosol jet printing of the micro-hotplate with silver ink have been tried as demonstrated in Figure 49 and Figure 50. Current results show that when applying voltage to the printed pattern, it would generate heat and elevate the temperature of the whole package. But after heating for some time, partial melting of the silver nanoparticles would happen which destroys the integrity of the conductive path. Figure 51 is an SEM image of part of the micro-hotplate after applying voltage.

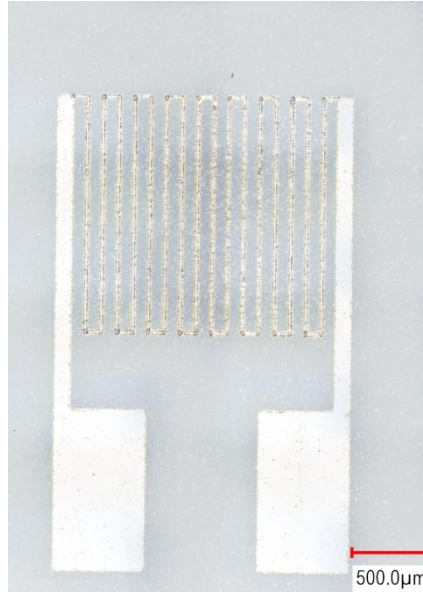


Figure 49 Micro-hotplate printed by silver ink with larger gaps

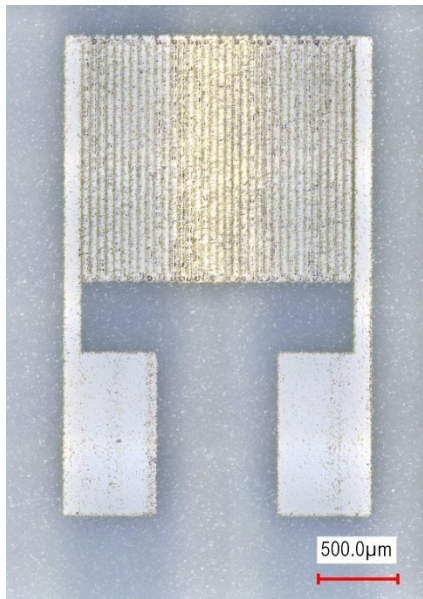


Figure 50 Micro-hotplate printed by silver ink with smaller gaps

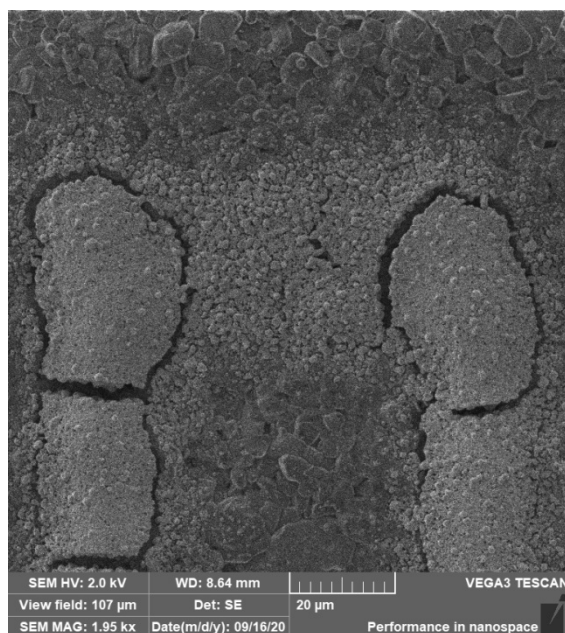


Figure 51 SEM image of the micro-hotplate after applying voltage

4.6.3 Sensing layers

Rectangles of 2 mm × 3.5 mm are printed as the sensing layer in the sensor package. For designing the CAD file, different gaps between lines have been tried in order to get the continuous and relatively smooth layer. If the gap is too large, the printed lines cannot overlap with each other, so that the formed layer is not continuous and could not achieve the correct electrical signal when sensing the chemicals. Figure 52 shows printed sensing layers with line gaps of 10 μm and 5 μm respectively. When the line gap is 10 μm, there are folds appearing on the layer surface. However, when the line gap is 5 μm, a smooth and flat layer could be produced. In the latter case, the surface roughness of the sensing layer is $1.3 \pm 0.1 \mu\text{m}$. For each sensing layer, the same pattern has been printed for 3 times, and the total thickness of the layer is 6 μm. For sensor testing, the pattern with the line gap of 5 μm is used for printing the

sensing layer. Figure 53 is the picture of the printed sensing layer, showing that the printed layer is transparent.

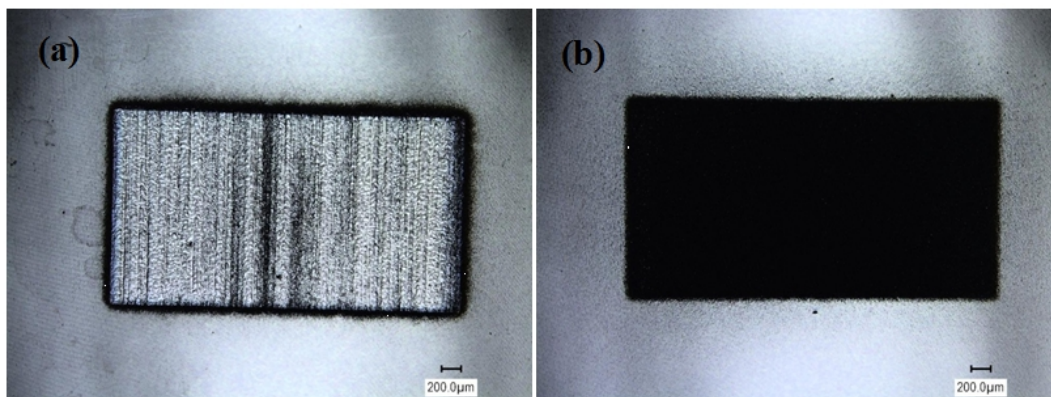


Figure 52 Printed sensing layer with designed gap of (a) 10 μm and (b) 5 μm

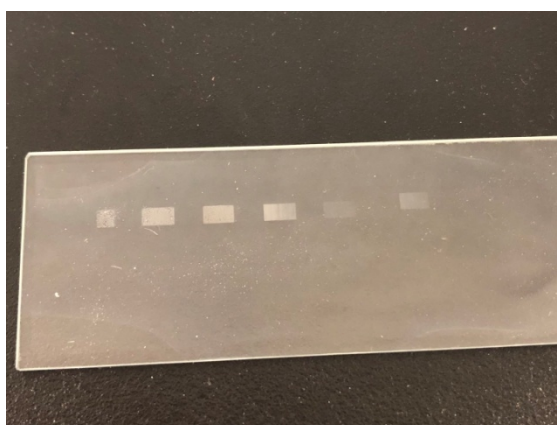


Figure 53 Cellphone picture of printed sensing layers on a glass slide

After annealing at 450 °C, microscope images are taken for another time, as shown in Figure 54. For the sensing layer with fold structures before annealing, heat treatment causes the film to shatter. Small fragments of materials form instead of a complete film. While for flat film before annealing, the integrity of the material could be achieved after heat treatment. The surface roughness of the flat sample measured after heat treatment is 0.21 μm.

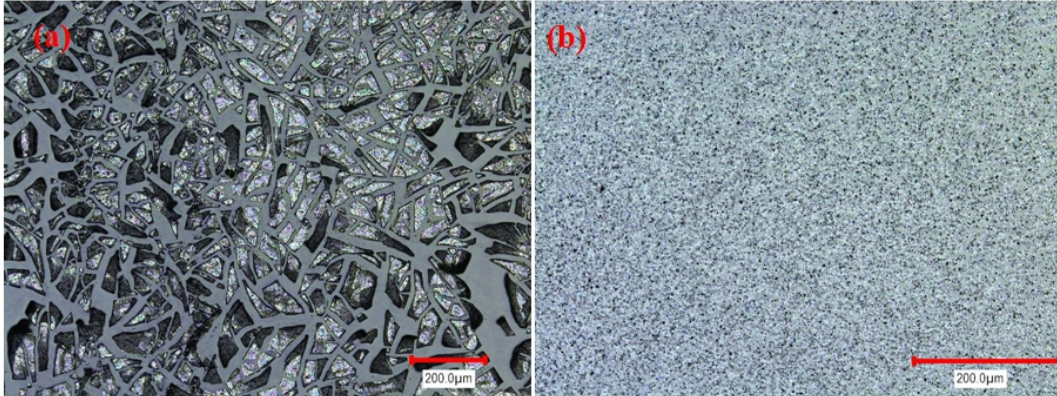


Figure 54 Optical image of sensing material after heat treatment

(a) fragments for sample with fold structure, (b) film integrity for sample with flat surface

Once achieving the printability of both electrodes and the sensing material, a combination of them is conducted, shown in Figure 55. The electrode with trace gap of 50 μm is selected and the sensing layer with the line gap of 5 μm is chosen.

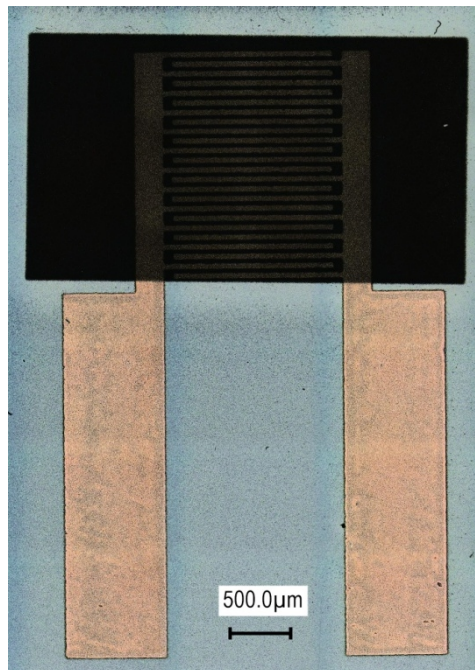


Figure 55 Printed sensing layer on the electrode with trace gap of 50 μm

4.7 Summary

In this chapter, the detailed processes for manufacturing tin oxide gas sensor package via aerosol jet printing are explained. In the first sections of this chapter, the structure of the printing system and important printing parameters that may influence the printing quality are introduced. Experiment is conducted to study the relationship between the printed line width and important printing parameters using silver ink as an example. The mixture of tin oxide sol solution and α -terpinol in a fixed volume ratio is used as the ink for printing sensing materials, while the commercial silver ink diluted with deionized water is applied to print electrodes and micro-hotplates. Functional parts printed with both inks are characterized via Keyence optical profilometer.

For improving gas sensing performance, the reduction of gap distance between conductive traces on the electrodes is significantly important. Experiments prove that aerosol jet printing has large potentials on effectively minimize the gap size without complicated masking steps. The electrodes with designed trace gap of 50 μm is used for the final sensor testing, with smaller actual gap of 39.12 μm due to the printed line width.

A trial on the fabrication of a micro-hotplate has been conducted as well. When applying a voltage to the micro-hotplate, it can generate some heat the raise the temperature of the sensor. However, after turning on the micro-hotplate for one time, cracks form on the material surface and damage the integrity and the conductivity.

In addition, the sensing material is printed with the sol solution and how the

pattern design would influence the printing quality is studied. When the line gap in the CAD pattern is too large, the resulted surface is not uniform. After heat treatment, shatters instead of a film form under the microscope view. Therefore, the gap between printed lines is optimized in order to achieve the integrity of the material and form a continuous conductive path.

Chapter 5 Summary and recommendations

In this chapter, the research project conducted in this thesis is summarized and important conclusions have been drawn. Both achievements of the thesis and disadvantages of the project are listed and described. Future work that can be conducted to improve the research qualities are stated as well.

5.1 Thesis summary

In this thesis, a gas sensor is fabricated via aerosol jet printing for acetone detection. Characterization work on both the sensing material and the sensor package have been done.

Sol gel technology is used for synthesizing sensing material. Thin film derived from the sol gel route has been characterized and the sensing performance has been tested using a home-built chamber. Results show that responses between 30 ppm and 1500 ppm are linear but the response time and recovery time of the sensor is not short enough. Factors that may affect repeatability and reproducibility of the study are analyzed.

Aerosol jet printing of electrodes, micro-hotplates and the sensing material is tried in this thesis. The advantage of aerosol jet printing on fabricating gas sensors is that it can easily adjust the pattern designs compared with photolithography. Electrodes with different trace gaps are manufactured and the one with the smallest gap is used for sensor testing. Micro-hotplates are tried with aerosol jet printing as well, but the pattern would be damaged after applying the voltage. Ink of sensing material is formulated and CAD design of the sensing layer is optimized in order to achieve the continuity of the printed layer.

As a summary, this thesis presents some preliminary results for fabricating gas sensors via micro-additive manufacturing used for detecting and monitoring acetone vapor. The results in the thesis prove the effectiveness of fabricating gas sensors using aerosol jet printing technique.

5.2 Achievements and disadvantages

Both achievements and disadvantages of this research are listed as follows.

Achievements:

1. The research presented in this thesis provides an alternative method for fabrication of gas sensors -- aerosol jet printing. Compared with other thin film technologies commonly used to make gas sensors, the advantage of aerosol jet printing lies in its flexibility to fabricate micro-/nano-electronics with complex geometry without complicated steps including masking. Also, it is possible to easily print the sensors on flexible substrates or substrates with curved shapes. The preliminary results in this thesis proves the feasibility of aerosol jet printing on manufacturing gas sensors.

2. The principles for designing and building a testing chamber for VOC gas sensors are described in detail in this thesis. For those who would like to do research work related to VOC sensors but do not have a professional testing system in the lab, the contents in this thesis may act as a reference on how to build a testing system.

3. In aerosol jet printing process, in order to print continuously, the ink should form stable mist in the ultrasonic atomizer. An aerosol jet printable tin oxide nanoparticle ink which could be atomized continuously is formulated in this research. The way and method of adjusting the ink in order to make the ink printable may provide a reference for those who would like to form aerosol jet printable inks from synthesized nanoparticles.

4. Principal printing parameters for aerosol jet printing systems that may affect

printing quality are studied using the example of silver ink. Also, relationship between CAD pattern design and printing quality is studied using the example of tin oxide nanoparticle ink. It gave us some thoughts that besides printing parameters and operation conditions of the machine, pattern design is another important influence factor in aerosol jet printing process. When designing the patterns, different line gaps should be used when printing with different inks.

Disadvantages:

1. Desired sensing performance is not achieved in this thesis. Since the main purpose for acetone sensors is to detect diabetes via breath analysis, the sensitivity of the sensor should be high enough and the response/recovery time should be short enough. Although the fabricated sensors in this thesis could achieve some response when exposing to acetone vapor, the detection limit is higher than expected. The response/recovery time of the sensor is long as well.

2. Since the testing chamber is designed and built in lab as a simple alternative to the professional testing system, and the environment with desired acetone concentration is generated by injecting acetone droplets or injecting high concentration of acetone vapor manually, the testing results for sensor response may not be so accurate.

3. For aerosol jet printing process, the ink condition varies with time, so it leads to the variation of printing qualities and properties of the printed sensors. Therefore, the sensitivity and the detection range of the printed sensors vary from each other.

5.3 Recommendations

In order to further study the acetone sensor behavior and improve the sensing response, some recommendations are listed as follows.

1. According to the current results, the response time of the sensor is too long. For the purpose of diabetes monitoring, the response time should be as short as possible. Therefore, effort should be put to minimize the sensor response and recovery time by addition of dopants or modifying the surface morphology.

2. Due to the lack of experimental equipments, low concentration of acetone vapor is not easy to generate. For achieving more accurate information about the sensing performance, tests should be done in professional gas testing systems.

3. Since the aim of the acetone sensor is to detect the acetone vapor concentration in human breath, the response change with the humidity is an important parameter. Thus, the sensing signal should be quantified as a function of the humidity.

4. For fabrication of micro-hotplates, suitable additives should be found to be added in the ink formulation to avoid cracks after applying voltage.

Letter of copyright permission

Among all the cited figures, Figure 2-4, 6-10 and 12-18 are reprinted from open access articles distributed under the terms and conditions of the Creative Commons Attribution license (<http://creativecommons.org/licenses/by/3.0/>).

Permissions and copyright for Figure 5, Figure 11 and Figure 25 are obtained from Copyright Clearance Center. Letters of copyright permission are as follows.




Analytical Investigation of Aerosol Jet Printing
Author: Sebastian Binder, , Markus Glatthaar, et al
Publication: Aerosol Science & Technology
Publisher: Taylor & Francis
Date: Sep 2, 2014
Rights managed by Taylor & Francis

Thesis/Dissertation Reuse Request

Taylor & Francis is pleased to offer reuses of its content for a thesis or dissertation free of charge contingent on resubmission of permission request if work is published.

[BACK](#) [CLOSE](#)

Permission for Figure 5



My Orders My Library My Profile Welcome manyou.sun@uwaterloo.ca Log out | Help

My Orders > Orders > All Orders

License Details

This Agreement between Ms. Manyou Sun ("You") and Elsevier ("Elsevier") consists of your license details and the terms and conditions provided by Elsevier and Copyright Clearance Center.

[Print](#) [Copy](#)

License Number	4999631189802
License date	Jan 31, 2021
Licensed Content Publisher	Elsevier
Licensed Content Publication	Materials Today: Proceedings
Licensed Content Title	Design and Simulation of MEMS Gas Sensor Topologies for Detection of Inert Gases
Licensed Content Author	Suma Umesh, T.C. Balachandra, A. Usha
Licensed Content Date	Jan 1, 2018
Licensed Content Volume	5
Licensed Content Issue	10
Licensed Content Pages	8
Type of Use	reuse in a thesis/dissertation
Portion	figures/tables/illustrations
Number of figures/tables/illustrations	1
Format	both print and electronic
Are you the author of this Elsevier article?	No
Will you be translating?	No
Title	Micro-Additive Manufacturing of Metal-Oxide-Semiconductor Based Gas Sensors for Diabetes Detection via Breath Analysis
Institution name	University of Waterloo
Expected presentation date	Feb 2021
Portions	Figure 1
Requester location	Ms. Manyou Sun

Permission for Figure 11

Transparent, Conducting ATO Thin Films by Epoxide-Initiated Sol-Gel Chemistry: A Highly Versatile Route to Mixed-Metal Oxide Films

Author: Matthias M. Koebel, Digambar Y. Nadargi, Giselle Jimenez-Cadena, et al

Publication: Applied Materials

Publisher: American Chemical Society

Date: May 1, 2012

Copyright © 2012, American Chemical Society



PERMISSION/LICENSE IS GRANTED FOR YOUR ORDER AT NO CHARGE

This type of permission/license, instead of the standard Terms & Conditions, is sent to you because no fee is being charged for your order. Please note the following:

- Permission is granted for your request in both print and electronic formats, and translations.
- If figures and/or tables were requested, they may be adapted or used in part.
- Please print this page for your records and send a copy of it to your publisher/graduate school.
- Appropriate credit for the requested material should be given as follows: "Reprinted (adapted) with permission from (COMPLETE REFERENCE CITATION). Copyright (YEAR) American Chemical Society." Insert appropriate information in place of the capitalized words.
- One-time permission is granted only for the use specified in your request. No additional uses are granted (such as derivative works or other editions). For any other uses, please submit a new request. If credit is given to another source for the material you requested, permission must be obtained from that source.

[BACK](#)

[CLOSE WINDOW](#)

Permission for Figure 25

References

- [1] TT Wohlers and W Associates, “WohlersReport 2020: 3D Printing and Additive Manufacturing State of the Industry,” *Wohlers Associates*, Ft. Collins, Co, 2020.
- [2] K. V. Wong and A. Hernandez, “A Review of Additive Manufacturing,” *ISRN Mech. Eng.*, vol. 2012, p. 208760, Aug. 2012.
- [3] ASTM International, *F2792-12a - Standard Terminology for Additive Manufacturing Technologies*. ASTM International, West Conshohocken, PA, 2013.
- [4] G. J. Marquez *et al.*, “Aerosol-Based Direct-Write of Biological Materials for Biomedical Applications,” *Mater. Res. Soc. Symp. Proc.*, vol. 698, no. 521, Mar. 2001.
- [5] J. M. Hoey *et al.*, “A Review on Aerosol-Based Direct-Write and its Applications for Microelectronics,” *J. Nanotechnol.*, vol. 2012, p. 324380, Sep. 2012.
- [6] N. J. Wilkinson *et al.*, “A review of Aerosol Jet Printing—a Non-Traditional Hybrid Process for Micro-Manufacturing,” *Int. J. Adv. Manuf. Technol.*, vol. 105, pp. 4599-4619, May 2019.
- [7] S. Binder *et al.*, “Analytical Investigation of Aerosol Jet Printing,” *Aerosol Sci. Technol.*, vol. 48, no. 9, pp. 924-929, Aug. 2014.
- [8] C. Goth *et al.*, “Aerosol Jet printing on Rapid Prototyping Materials for Fine Pitch Electronic Applications,” in *2011 IEEE 61st Electronic Components and Technology Conference (ECTC)*, Lake Buena Vista, FL, 2011, pp. 1211-1216.
- [9] R. Salary *et al.*, “A Computational Fluid Dynamics (CFD) Study of Pneumatic

- Atomization in Aerosol Jet Printing (AJP) Process,” in *ASME International Mechanical Engineering Congress and Exposition, Proceedings (IMECE)*, Salt Lake City, UT, 2019.
- [10] R. Salary *et al.*, “Computational Fluid Dynamics Modeling and Online Monitoring of Aerosol Jet Printing Process,” *J. Manuf. Sci. Eng. Trans. ASME*, vol. 139, no. 2, p. 021015, Feb. 2017.
- [11] S. Agarwala *et al.*, “Wearable Bandage-Based Strain Sensor for Home Healthcare: Combining 3D Aerosol Jet Printing and Laser Sintering,” *ACS Sensors*, vol. 4, no. 1, pp. 218-226, Dec. 2019.
- [12] K. T. Fujimoto *et al.*, “Aerosol Jet Printed Capacitive Strain Gauge for Soft Structural Materials,” *npj Flex. Electron.*, vol. 4, no. 32, pp. 1-9, Nov. 2020.
- [13] D. Zhao *et al.*, “Fabrication and Characterization of Aerosol-Jet Printed Strain Sensors for Multifunctional Composite Structures,” *Smart Mater. Struct.*, vol.21, p. 115008, Sep. 2012.
- [14] A. A. Vasiliev *et al.*, “Aerosol/Ink Jet Printing Technology for High-Temperature MEMS Sensors,” *Proceedings*, vol. 1, no. 4, p. 617, Aug. 2017.
- [15] Y. Zhu *et al.*, “A High-Sensitivity Graphene Ammonia Sensor via Aerosol Jet Printing,” *Sensors Actuators, A Phys.*, vol. 318, p. 112434, Dec. 2021.
- [16] R. Liu *et al.*, “Fabrication of Platinum-Decorated Single-Walled Carbon Nanotube Based Hydrogen Sensors by Aerosol Jet Printing,” *Nanotechnology*, vol. 23, no. 50, p. 505301, Nov. 2012.
- [17] L. Tu *et al.*, “Aerosol Jet Printed Silver Nanowire Transparent Electrode for

- Flexible Electronic Application,” *J. Appl. Phys.*, vol. 123, no. 17, p. 174905, May 2018.
- [18] H. Alemohammad *et al.*, “A Dual-Parameter Optical Fiber Sensor for Concurrent Strain and Temperature Measurement: Design, Fabrication, Packaging and Calibration,” *J. Lightw. Technol.*, vol. 31, no. 8, pp. 1198-1204, Apr. 2013.
- [19] H. Alemohammad and E. Toyserkani, “Simultaneous Measurement of Temperature and Tensile Loading Using Tunable Superstructure FBGs Developed by Laser-Direct Writing of Periodic On-Fiber Metallic Films,” *Smart Mater. Struct.*, vol. 18, no. 9, p. 095048, Aug. 2009.
- [20] X. Zhang *et al.*, “Sensitivity Alteration of Fiber Bragg Grating Sensors with Additive Micro-Scale Bi-Material Coatings,” *Meas. Sci. Technol.*, vol. 24, no. 2, p. 025106, Jan. 2013.
- [21] H. Alemohammad and E. Toyserkani, “Metal Embedded Optical Fiber Sensors: Laser-Based Layered Manufacturing Procedures,” *J. Manuf. Sci. Eng.*, vol. 133, no. 3, p. 031015-1, Jun. 2011.
- [22] E. Foroozmehr *et al.*, “Laser Assisted Surface Patterning of Magnesium with Silver Nanoparticles: Synthesis, Characterization and Modeling,” *J. Phys. D Appl. Phys.*, vol. 44, no. 49, p. 495305, Nov. 2011.
- [23] E. Jabari and E. Toyserkani, “Micro-Scale Aerosol-Jet Printing of Graphene Interconnects,” *Carbon*, vol. 91, pp. 321-329, May. 2015.
- [24] E. Jabari and E. Toyserkani, “Laser Heat Treatment of Aerosol-Jet Additive Manufactured Graphene Patterns,” *J. Phys. D Appl. Phys.*, vol. 48, no. 37, p.

275503, Aug. 2015.

- [25] G. Korotcenkov, *Handbook of Gas Sensor Materials*. New York: Springer, 2014.
- [26] A. Hulanicki *et al.*, “Chemical Sensors: Definitions and Classification,” *Pure & Appl. Chem.*, vol. 63, no. 9, pp. 1247-1250, 1991.
- [27] A. Mirzaei *et al.*, “Detection of Hazardous Volatile Organic Compounds (VOCs) by Metal Oxide Nanostructures-Based Gas Sensors: A Review,” *Ceramics International*, vol. 42, no. 14, pp. 15119-15141, Nov. 2016.
- [28] C. Wang *et al.*, “Metal Oxide Gas Sensors: Sensitivity and Influencing Factors,” *Sensors*, vol. 10, no. 3, pp. 2088-2106, Mar. 2010.
- [29] V. Dobrokhotov *et al.*, “Vapor Trace Recognition Using a Single Nonspecific Chemiresistor,” *Sensors (Basel)*, vol. 13, no. 7, pp. 9016-9028, Jul. 2013.
- [30] Y. F. Sun *et al.*, “Metal Oxide Nanostructures and Their Gas Sensing Properties: A Review,” *Sensors*, vol. 12, no. 3, pp. 2610-2631, Feb. 2012.
- [31] S. Umesh *et al.*, “Design and Simulation of MEMS Gas Sensor Topologies for Detection of Inert Gases,” *Mater. Today Proc.*, vol. 5, no. 10, p. 1, pp. 21355-21362, Oct. 2018.
- [32] V. M. Aroutiounian, “Acetone Sensor Made of Tin Dioxide,” *J. Contemp. Phys.*, vol. 55, no.3, pp. 213-224, Sep. 2020.
- [33] M. M. Zhang and G. S. Jiang, “Gas Sensing Properties of Co_3O_4 -Loaded SnO_2 to Ethanol and Acetone,” *Chinese J. Chem. Phys.*, vol. 20, no. 3, pp. 315-318, Sep. 2007.
- [34] Y. Zhang *et al.*, “Gas Sensor Based on Samarium Oxide Loaded

- Mulberry-Shaped Tin Oxide for Highly Selective and Sub ppm-Level Acetone Detection,” *J. Colloid Interface Sci.*, vol. 531, pp. 74-82, Jul. 2018.
- [35] W. Q. Li *et al.*, “Synthesis of Hollow SnO₂Nanobelts and Their Application in Acetone Sensor,” *Mater. Lett.*, vol. 132, pp. 338-341, Jun. 2014.
- [36] T. T. Wang *et al.*, “Facile Fabrication of Multishelled SnO₂Hollow Microspheres for Gas Sensing Application,” *Mater. Lett.*, vol. 164, pp. 56-59, Oct. 2016.
- [37] Q. Wang *et al.*, “Enhanced Gas Sensing Properties of Hierarchical SnO₂Nanoflower Assembled from Nanorods via a One-Pot Template-Free Hydrothermal Method,” *Ceram. Int.*, vol. 42, no. 14, pp. 15889-15896, Jul. 2016.
- [38] A. V. Nikam *et al.*, “Wet Chemical Synthesis of Metal Oxide Nanoparticles: A Review,” *CrystEngComm*, vol. 20, no. 35, pp. 5091-5107, Jul. 2018.
- [39] B. L. Cushing *et al.*, “Recent Advances in the Liquid-Phase Syntheses of Inorganic Nanoparticles,” *Chem. Rev.*, vol. 104, no. 9, pp. 3893-3946, Aug. 2004.
- [40] Ebelmen, “Untersuchungen über die Verbindungen der Borsäure und Kieselsäure mit Aether,” *Justus Liebigs Ann. Chem.*, vol. 57, no. 3, pp. 319-355, 1846.
- [41] L. L. Hench and J. K. West, “The Sol-Gel Process,” *Chem. Rev.*, vol. 90, no. 1, pp. 33-72, 1990.
- [42] W. Geffcken and E. Berger, “Verfahren zur Änderung des Reflexionsvermögens optischer Gläser,” German Patent 736 411, May 1939.
- [43] T. Graham, “On the Properties of Silicic Acid and Other Analogous Colloidal Substances,” *J. Chem. Soc.*, vol. 17, pp. 318-327, 1864.

- [44] C. B. Hurd, "Theories for the Mechanism of the Setting of Silicic Acid Gels," *Chem. Rev.*, vol. 22, no. 3, pp. 403-422, Jun. 1938.
- [45] D. M. Roy and R. Roy, "An Experimental Study of the Formation and Properties of Synthetic Serpentine and Related Layer Silicate Minerals," *Amer. Miner.*, vol. 39, no. 11-12, pp. 957-975, Dec. 1954.
- [46] R. Roy, "Gel Route to Homogeneous Glass Preparation," *J. Am. Ceram. Soc.*, vol. 52, no. 6, pp. 344-344, Jun. 1969.
- [47] H. Dislich, "New Routes to Multicomponent Oxide Glasses," *Angew. Chemie Int. Ed. English*, vol. 10, no. 6, pp. 363-370, Jun. 1971.
- [48] C. J. Brinker and G. W. Scherer, *Sol-Gel Science: The Physics and Chemistry of Sol-Gel Processing*. Academic Press, 2013.
- [49] B. E. Yoldas, "Preparation of Glasses and Ceramics from Metal-Organic Compounds," *J. Mater. Sci.*, vol. 12, pp. 1203-1208, Jun. 1977.
- [50] D. H. Everett, "Manual of Symbols and Terminology for Physicochemical Quantities and Units, Appendix II: Definitions, Terminology and Symbols in Colloid and Surface Chemistry," in *Pure and Applied Chemistry*, 2019.
- [51] J. Alemán *et al.*, "Definitions of Terms Relating to the Structure and Processing of Sols, Gels, Networks, and Inorganic-Organic Hybrid Materials (IUPAC Recommendations 2007)," *Pure Appl. Chem.*, 2007.
- [52] A. E. Danks *et al.*, "The Evolution of 'Sol-Gel' Chemistry as a Technique for Materials Synthesis," *Mater. Horiz.*, vol. 3, no. 2, pp. 91-112, 2016.
- [53] P. Innocenzi, *The Sol-to-Gel Transition*. Cham: Springer Nature Switzerland

AG,2019.

- [54] M. N. Rahaman, *Ceramic Processing and Sintering*. CRC Press, 2017.
- [55] A. Mujahid *et al.*, “Chemical Sensors Based on Molecularly Imprinted Sol-Gel Materials,” *Materials.*, vol. 3, no. 4, pp. 2196-2217, Mar. 2010.
- [56] F. B. M. Suah *et al.*, “Applications of Artificial Neural Network on Signal Processing of Optical Fibre pH Sensor Based on Bromophenol Blue Doped with Sol-Gel Film,” *Sens. Actuators B Chem.*, vol. 90, no. 1-3, pp. 182-188, Apr. 2003.
- [57] H. Gullapalli *et al.*, “Flexible Piezoelectric ZnO-Paper Nanocomposite Strain Sensor,” *Small*, vol. 6, no. 15, pp. 1641-1646, Aug. 2010.
- [58] A. Z. Adamyan *et al.*, “Sol-Gel Derived Thin-Film Semiconductor Hydrogen Gas Sensor,” *Int. J. Hydrogen Energy*, vol. 32, no. 16, pp. 4101-4108, Nov. 2007.
- [59] D. B. Mahadik *et al.*, “Effect of Water Ethanol Solvents Mixture on Textural and Gas Sensing Properties of Tin Oxide Prepared Using Epoxide-Assisted Sol-Gel Process and Dried at Ambient Pressure,” *Solid State Sci.*, vol. 50, pp. 1-8, Oct. 2015.
- [60] L. Pauling *et al.*, “Quantitative Analysis of Urine Vapor and Breath by Gas-Liquid Partition Chromatography,” *Proc. Natl. Acad. Sci. U. S. A.*, vol. 68, no. 10, pp. 2374-2376, Oct. 1971.
- [61] T. A. Popov, “Human exhaled breath analysis,” *Annals of Allergy, Asthma and Immunology.*, vol. 106, no. 6, pp. 451-456, Jun. 2011.
- [62] B. Buszewski *et al.*, “Human Exhaled Air Analytics: Biomarkers of Diseases,”

- Biomed.Chromatogr.*, vol. 21, no. 6, pp. 553-566, Jun. 2007.
- [63] T. D. C. Minh *et al.*, “The Clinical Potential of Exhaled Breath Analysis for Diabetes Mellitus,” *Diabetes Res. Clin.Pract.*,vol. 97, no. 2, pp. 195-205, Aug. 2012.
- [64] T. Mathew *et al.*, “Technologies for Clinical Diagnosis Using Expired Human Breath Analysis,” *Diagnostics*, vol. 5, no. 1, pp. 27-60, Feb. 2015.
- [65] M. P. Kalapos, “On the Mammalian Acetone Metabolism: From Chemistry to Clinical Implications,” *Biochim.Biophys. Acta.*, vol. 1621, no. 2, pp. 122-139, May 2003.
- [66] K. K. Dhillon and S. Gupta, *Biochemistry, Ketogenesis*. Treasure Island: StatPearls, 2018.
- [67] Z. Wang and C. Wang, “Is Breath Acetone a Biomarker of Diabetes? A Historical Review on Breath Acetone Measurements,” *J. Breath Res.*, vol. 7, no. 3, p. 037109, Sep. 2013.
- [68] M. J. Henderson *et al.*, “Acetone in the Breath; a Study of Acetone Exhalation in Diabetic and Nondiabetic Human Subjects,” *Diabetes.*, vol. 1, no. 3, pp. 188-193, May-Jun. 1952.
- [69] G. Rooth and S. Ostenson, “Acetone in Alveolar Air, and the Control of Diabetes.,” *Lancet.*, vol. 2, no. 7473, pp. 1102-1105, Nov. 1966.
- [70] C. N. Tassopoulos *et al.*, “Breath-Acetone and Blood-Sugar Measurements in Diabetes.,” *Lancet*, vol. 1, no. 7609, pp. 1282-1286, Jun. 1969.
- [71] N. Nelson *et al.*, “Exhaled Isoprene and Acetone in Newborn Infants and in

- Children with Diabetes Mellitus,” *Pediatr. Res.*, vol. 44, pp. 363-367, Sep. 1998.
- [72] C. Turner *et al.*, “Breath Acetone Concentration Decreases with Blood Glucose Concentration in Type I Diabetes Mellitus Patients during Hypoglycaemic Clamps,” *J. Breath Res.*, vol. 3, no. 4, p. 046004, Dec. 2009.
- [73] C. Deng *et al.*, “Determination of Acetone in Human Breath by Gas Chromatography–Mass Spectrometry and Solid-Phase Microextraction with On-Fiber Derivatization,” *J. Chromatogr. B*, vol. 810, no. 2, pp. 269-275, Oct. 2004.
- [74] M. B. Greiter *et al.*, “Differences in Exhaled Gas Profiles between Patients with Type 2 Diabetes and Healthy Controls,” *Diabetes Technol. Ther.*, vol. 12, no. 6, pp. 455-463, Jun. 2010.
- [75] J. Lisec *et al.*, “Gas Chromatography Mass Spectrometry-Based Metabolite Profiling in Plants,” *Nat. Protoc.*, vol. 1, pp. 387-396, Jun. 2006.
- [76] A. Amann *et al.*, “Model Based Determination of Detection Limits for Proton Transfer Reaction Mass Spectrometer,” *Meas. Sci. Rev.*, vol. 10, no. 6, pp. 180-188, Dec. 2010.
- [77] D. Smith and P. Španěl, “Ambient Analysis of Trace Compounds in Gaseous Media by SIFT-MS,” *Analyst.*, vol. 136, no. 10, pp. 2009-2032, Mar. 2011.
- [78] C. Wang *et al.*, “A Study on Breath Acetone in Diabetic Patients Using a Cavity Ringdown Breath Analyzer: Exploring Correlations of Breath Acetone with Blood Glucose and Glycohemoglobin A1C,” *IEEE Sens. J.*, vol. 10, no. 1, pp. 54-63, Jan. 2010.

- [79] G. Eranna *et al.*, "Oxide Materials for Development of Integrated Gas Sensors - A Comprehensive Review," *Crit. Rev. Solid State Mater. Sci.*, vol. 29, no. 3-4, pp. 111-188, Aug. 2004.
- [80] M. A. Basyooni *et al.*, "Structural, Optical, Electrical and Room Temperature Gas Sensing Characterizations of Spin Coated Multilayer Cobalt-Doped Tin Oxide Thin Films," *Superlattices Microstruct.*, vol. 140, p. 106465, Apr. 2020.
- [81] M. M. Koebel *et al.*, "Transparent, Conducting ATO Thin Films by Epoxide-Initiated Sol-Gel Chemistry: A Highly Versatile Route to Mixed-Metal Oxide Films," *ACS Appl. Mater. Interfaces*, vol. 4, no. 5, pp. 2464-2473, Apr. 2012.
- [82] P. Si *et al.*, "Dual Colorimetric and Conductometric Responses of Silver-Decorated Polypyrrole Nanowires for Sensing Organic Solvents of Varied Polarities," *ACS Appl. Mater. Interfaces*, vol. 10, no. 35, pp. 29227-29232, Aug. 2018.
- [83] S. F. Bamsaoudet *al.*, "Nano Particulate SnO₂ Based Resistive Films as a Hydrogen and Acetone Vapour Sensor," *Sens. Actuators B Chem.*, vol. 153, no. 20, pp. 382-391, Apr. 2011.